DIGITAL ACCESS TO SCHOLARSHIP AT HARVARD
DASH.HARVARD.EDU

HARVARD LIBRARY

Bistable dynamics in microbial ecology and systems biology

Citation
Axelrod, Kevin Connor. 2016. Bistable dynamics in microbial ecology and systems biology. Doctoral dissertation, Harvard University, Graduate School of Arts & Sciences.

Link
http://nrs.harvard.edu/urn-3:HUL.InstRepos:33493470

Terms of use
This article was downloaded from Harvard University's DASH repository, and is made available under the terms and conditions applicable to Other Posted Material (LAA), as set forth at
https://harvardwiki.atlassian.net/wiki/external/NGY5NDE4ZjgzNTc5NDQzMGIzZWZhMGFlOWI2M2EwYTg

Accessibility
https://accessibility.huit.harvard.edu/digital-accessibility-policy

Share Your Story
The Harvard community has made this article openly available.
Please share how this access benefits you. Submit a story

Bistable dynamics in microbial ecology and systems biology

A dissertation presented

by

Kevin Connor Axelrod

to

The Committee on Higher Degrees in Biophysics

in partial fulfillment of the requirements

for the degree of

Doctor of Philosophy

in the subject of

Biophysics

Harvard University

Cambridge, Massachusetts

April 2016

© 2016 Kevin Connor Axelrod

All rights reserved.

Dissertation Advisor: Dr. Jeff Gore Kevin Connor Axelrod

Bistable dynamics in microbial ecology and systems biology

Abstract

Bistability, in which a system has two stable states, is a common property of many dynamic systems. This thesis explores the properties of such systems across a range of length scales, from gene circuits to ecosystems. Cells often store memories of environmental stimuli using bistable gene circuits. High fidelity memory storage requires that a state has a long lifetime. However, an underappreciated aspect of stable memory is that the distance from a bifurcation could determine how sensitive a state is to perturbations in the extracellular environment. We predict that cell memory should become increasingly sensitive to perturbations near a bifurcation and test this idea in three different gene circuits: a toggle switch, the yeast galactose utilization network, and the *E. coli* lactose utilization network.

In a second study, we explore how the environmental context in which two species interact can influence their mode of interaction. Two species in nature often form reciprocally beneficial partnerships termed mutualisms, but in certain environmental regimes the species might shift to competing with one another for resources. This mutualism-competition transition has been understudied in experimental ecosystems. Using a synthetic yeast cross-feeding mutualism, we modulate the degree to which two partners rely on each other by supplementing the cells with variable amounts of nutrients. Surprisingly, we find that as the amount of supplemented nutrients is increased, the system passes through eight qualitatively distinct dynamic regimes: extinction, obligatory mutualism, obligatory/facultative mutualism, facultative mutualism, parasitism, amensalism, competition, and competitive exclusion.

In a third study, we probe how population growth dynamics can influence the probability of evolutionary rescue. Natural populations frequently face harsh environments in which their death rate exceeds their birth rate and population size tends toward zero. In such scenarios, populations can either go extinct, migrate to a better habitat, or adapt to the harsh environment. Natural populations often exhibit an "Allee effect," in which populations grow slowly at low density due to struggles with such behaviors as finding a mate or collective hunting. We hypothesize that the presence of an Allee effect could impede evolutionary rescue and confirm this hypothesis in a model laboratory yeast ecosystem.

Table of Contents

1. Critical Transitions in Gene Networks
    1. Background and Motivation
    2. Cell Memory in the Toggle Switch
    3. Resilience to Directional Perturbations
    4. Resilience to Generic Perturbations
    5. Mapping the Bifurcation Diagram
    6. Generic Early Warning Indicators of Critical Transition
    7. Yeast GAL and *E. coli* Lactose Networks
    8. Discussion
    9. Appendix
2. Yeast Cross-feeding Mutualism Dynamics
    1. Background and Motivation
    2. Synthetic Obligatory Mutualism in Batch Culture
    3. Phenomenological Model of Mutualism
    4. Testing the Predictions of the Model
    5. Characteristic Behavior Before Population Collapse
    6. Discussion
    7. Appendix
3. The Allee Effect and Evolutionary Rescue
    1. Background and Motivation
    2. Computational Simulations
    3. Experiments in Glucose and Sucrose
    4. Reinoculation Experiments
    5. Discussion
    6. Appendix
4. Conclusion
    1. Side Projects
    2. Future Directions
5. References

List of Figures

1.1 Memory in the toggle switch
1.2 Lifetimes of the stable states
1.3 Switching kinetics are non-exponential
1.4 Gating to control for cell size
1.5 Resilience of GFP state to directional perturbations
1.6 Resilience of RFP state to directional perturbations
1.7 Resilience of GFP state to generic perturbations
1.8 Switching increases with perturbation intensity
1.9 Generic perturbation results are reproducible
1.10 Resilience of RFP state to generic perturbations
1.11 Mapping the bifurcation
1.12 Computational modeling to understand basin boundary
1.13 Switching paths between stable states
1.14 Early warning indicators of bifurcation
1.15 Yeast GAL network experiments
1.16 *E. coli* lactose network experiments
1.17 Minimum perturbation duration to induce switching
1.18 Not all perturbations induce switching
2.1 Experimental demonstration of cross-feeding mutualism
2.2 Relative fitness of two strains
2.3 Computational model of mutualism dynamics
2.4 Monoculture and co-culture dynamics in different environments
2.5 Different qualitative regimes measured experimentally
2.6 Determining equilibrium cell concentrations
2.7 Eigenvector and eigenvalues determined computationally
2.8 Different paths to the stable fixed point
2.9 Growth curves before and after adaptation
2.10 Dynamics with non-producer and double-producer
2.11 Phase diagram varying amino acids and death rate
3.1 Survival dynamics in glucose and sucrose
3.2 Tau-leaping simulations
3.3 Cells in glucose transition from survival to rescue to extinction
3.4 Cells in sucrose go extinct where cells in glucose undergo rescue
3.5 Fate of populations depends on how fast growth curve shifts
3.6 Reinoculation experiments
4.1 Mutual invasibility of pure strategists
4.2 Relative fitness in semi-continuous environment
4.3 Evolution of mixed strategy from pure strategy

Acknowledgements

When I embarked on this adventure five years ago, I was forewarned that graduate school would be a challenging, stressful, and depressing period of my life. Thankfully, my experience at Harvard/MIT has been fantastic. I have simply adored the freedom to explore interesting questions, design fun experiments, and learn from brilliant people.

Thank you to Professor Jeff Gore for providing me with countless hours of mentoring and support. You somehow manage to strike the perfect balance between giving guidance when it is needed while also giving me the opportunity to learn from my own mistakes. It has been a pleasure watching the lab evolve during the last four years, and I can't wait to come to your tenure talk this fall.

Thank you to several people at Harvard for graciously donating their time to guide me through the degree process by serving on my qualifying exam committee, my dissertation advisory committee, and/or my thesis exam committee: Catherine Dulac, Joe Avruch, Brendan Manning, Allon Klein, Mike Springer, Andrew Murray, and Adam Cohen.

Thank you to Jim Hogle and Michele Jakoulov for overseeing the best graduate program at Harvard and for letting me tailor my coursework and research to my future career goals.

Thank you to members of the Gore lab for many fun ski trips, beach trips, journal clubs, and group meetings. I will miss serving as your "fun czar" and "snack fairy." A special thanks to Eugene Yurtsev for spending countless hours fixing my MATLAB code and for playing way too many games of ping pong with me.

Thank you to Sam Freeman, Nate Roquet, and Steph Hays for making my life outside the lab much more fun. In the words of Kelly Clarkson, "my life would suck without you." Thank you to Emily Mayer and my family for your love and support during this unforgettable journey.

Cambridge, MA Kevin Connor Axelrod

Introduction

This is a thesis which uses laboratory yeast to probe questions drawn from the fields of systems biology and theoretical ecology. A unifying feature of these studies is a focus on bistable dynamic systems across a range of length scales, from gene circuits to ecosystems. Many dynamic systems researchers have sought "generic" early warning indicators of an impending bifurcation. Such indicators would be useful because bifurcations in complex systems (such as collapse of ecosystems or financial markets) can occur suddenly and can be very hard to reverse once they occur. Whether or not such metrics will be useful tools in predicting bifurcations in real-world systems remains an open question.

In the first chapter, we use a toggle switch as a model for cell memory. We find that when cells are prepared in either a high Lac state or high Tet state and then transferred to an intermediate concentration of small molecule inducer, the system displays remarkably stable memory. However, we show that near a bifurcation, temporary perturbations in the environment (such as a heat or salt shock) can cause many cells to switch from the memory state into an alternative phenotypic state. We use the perturbation experiments to locate the unstable fixed points and construct a bifurcation diagram of the system. We observe qualitatively similar results in both the yeast galactose and *E. coli* lactose utilization networks. Intriguingly, we find that early warning indicators based on critical slowing down fail to predict the approaching bifurcation in the toggle switch.

In chapters two and three, we move from systems biology to ecological dynamics, where our key questions revolve around how population sizes evolve in time. In chapter two, we probe the mutualism-competition transition in a synthetic microbial cross-feeding mutualism. Adjusting the amount of supplemented amino acids in the growth media provides a remarkably

simple knob for tuning the degree to which the two partners in a mutualism require each other for growth. By characterizing the strains in monoculture and co-culture, we show that the system passes through eight qualitatively distinct regimes: extinction, obligatory mutualism, obligatory/facultative mutualism, facultative mutualism, parasitism, amensalism, competition, and competitive exclusion.

We close with some preliminary results on a study of how yeast populations alter their genetic structure to avert extinction in harsh environments. Evolutionary rescue will be increasingly important in ecology due to anthropogenic climate change, which is forcing species to go extinct at alarming rates. However, as a population declines in size in a harsh environment, it may fall into a regime of low growth rate caused by cooperative growth dynamics. The presence of a strong Allee effect in a population could dramatically hinder evolutionary rescue, yet this fact has been underappreciated in ecology. We use glucose and sucrose metabolism to tune the degree of cooperativity in a population and show that populations in sucrose are less likely to undergo evolutionary rescue.

The work described in this thesis can be found in the following publications:

- Axelrod, Sanchez, and Gore, *eLife* 2015
- Hoek, Axelrod, Biancalani, Yurtsev, Liu, and Gore, *under review at PLOS Biology*
- Healey, Axelrod, and Gore *in revision at Molecular Systems Biology*
- Axelrod, Shi, and Gore, *in progress*

Chapter 1

Critical Transitions in Gene Circuits

Microorganisms often exhibit a history-dependent phenotypic response after exposure to a stimulus which can be imperative for proper function. However, cells frequently experience unexpected environmental perturbations that might induce phenotypic switching. How cells maintain phenotypic states in the face of environmental fluctuations remains an open question. Here, we use environmental perturbations to characterize the resilience of phenotypic states in a synthetic gene network near a critical transition. We find that far from the critical transition an environmental perturbation may induce little to no phenotypic switching, whereas close to the critical transition the same perturbation can cause many cells to switch phenotypic states. This loss of resilience was observed for perturbations that interact directly with the gene circuit as well as for a variety of generic perturbations—such as salt, ethanol, or temperature shocks—that alter the state of the cell more broadly. We obtain qualitatively similar findings in natural gene circuits, such as the yeast GAL network. Our findings illustrate how phenotypic memory can become destabilized by environmental variability near a critical transition.

1.1 Background and motivation

Microbes such as yeast and bacteria often adopt a specific phenotype in response to an environmental stimulus, and in many cases this phenotype can be retained even after the stimulus has been removed[1–4]. Stably storing such a phenotype can be critical for survival during adverse environmental changes[5–8]. Several well-studied natural gene networks can be found in multiple phenotypic states depending on the history that the cells have experienced, notably including the yeast galactose utilization network and sporulation commitment in *B. Subtilis*[4,9]. Additionally,

synthetic biology aims to create de novo phenotypic memory storage devices, which could be used in applications such tracking dynamics of the gut microbiome[10,11]. In spite of the importance of phenotypic memory in natural and synthetic gene circuits, little is known about how environmental perturbations might disrupt a cell's ability to stably adopt a phenotype.

Given that phenotypic memory often results from feedback loops within the cell[3,12–15], it is possible that this phenotypic memory will display characteristics of other complex systems that exhibit bistability, memory, and associated critical transitions or "tipping points" that lead to sudden changes in the state of the system in response to small changes in the environment. A phenomenon that may be especially relevant to cellular memory is that complex systems near a critical transition experience a loss of resilience of their stable states to external perturbations[16]. In particular, a system far from a critical transition may return to its original state following a perturbation, whereas closer to the critical transition the same environmental perturbation may cause the system to switch to an alternative stable state (e.g. collapse of a population[16]). The dynamics in the vicinity of the critical point are very slow on both sides of the critical point. Therefore, it is worth noting that a short lived perturbation that pushes the system past the critical point may also not cause switching if the perturbation is short enough, if it pushes it to a position that is close to the critical point, or both. This aforementioned loss of resilience near a critical transition results from a shrinking basin of attraction in the stability landscape[17]. In the context of a gene network, this loss of resilience would manifest as a loss of phenotypic memory against environmental perturbations approaching the environmental condition in which cells would (deterministically) switch to a different phenotype. Our initial goal was to observe memory in a model gene circuit and then characterize the resilience of the phenotypic state against perturbations in the extracellular environment.

1.2 Cell Memory in the Toggle Switch

To study this predicted loss of resilience, we first employed a synthetic genetic switch in budding yeast that has previously been shown to exhibit hysteresis and bistability[18–21]. This toggle switch is composed of two mutually inhibitory transcription factors, LacI and TetR (Figure 1.1A). To enable tracking of the state of the cell, different color fluorescent proteins are expressed depending upon which of these transcriptional factors is highly expressed (mCherry and eGFP, hereafter referred to as "RFP" and "GFP"). As external knobs to control the state of the cell, the inducer IPTG modulates the strength of repression of LacI, whereas ATc modulates the strength of repression of TetR.

As a demonstration of how cellular memory operates in this gene network, one population of cells was pre-grown in IPTG to initialize the cells in a high GFP state (Figure 1.1B). A separate population of cells was pre-grown in ATc to initialize the cells in a high RFP state. We then transferred the populations to a range of ATc concentrations and monitored the dynamics over several days using flow cytometry. All cultures were grown with a fixed concentration of IPTG (40 μM), which served as an orthogonal control variable for later experiments. For high and low concentrations of ATc, cells converged to a state that was independent of the history they were pre-grown in (Figure 1.1, B and C). However, for intermediate concentrations of ATc there was little to no switching of the phenotypic state of the cells even after 260 hours of growth and over 80 cell divisions. The mutual repression in this toggle switch therefore indeed allows for remarkably stable cellular memory for intermediate ATc concentrations. As expected[4], the lifetime of the state decreases approaching the critical transition at which switching is deterministic (hereafter, we refer to this point as the "critical transition" or "phenotypic switch"), although interestingly we observe non-exponential switching

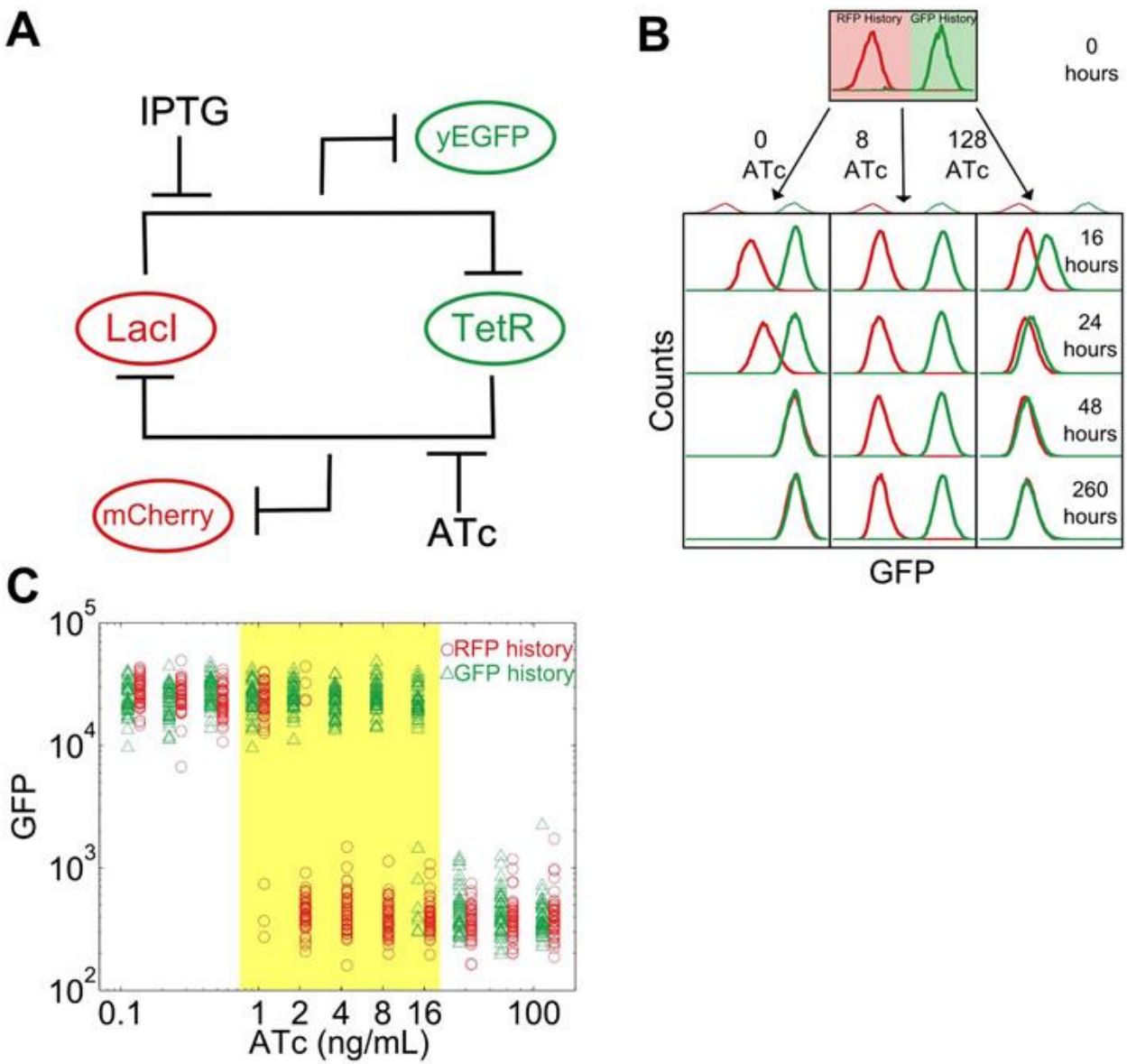

Figure 1.1: A toggle switch in yeast exhibits hysteresis and bistability.

(**A**) A toggle switch consists of two mutually inhibitory transcription factors, two fluorescent readouts of the system state, and two small molecule inhibitors of the transcription factors. (**B**) Following growth in one of two histories, cells are then diluted into a range of ATc concentrations and propagated in culture for several days. Histogram counts are binned logarithmically. (**C**) The intensity of GFP fluorescence is plotted as a function of [ATc] for 11 different conditions for the high GFP history (green triangles) and high RFP history (red circles) after 92 hr of growth. The distributions are offset for ease of viewing. 20,000 events are collected, and then a narrow gate is drawn to select several hundred cells of roughly equal size. From this narrow gate, 50 cells at random are plotted. The region of memory is shaded in yellow.

kinetics, potentially indicating the presence of metastable states in the gene network (Figure 1.2 and Figure 1.3). This decrease in lifetime is one manifestation of deteriorating cellular memory approaching the critical transition, but it is not obvious whether in ATc concentrations with long lifetimes (i.e. strong memory) the cells are also able to retain their memory in the face of environmental perturbations.

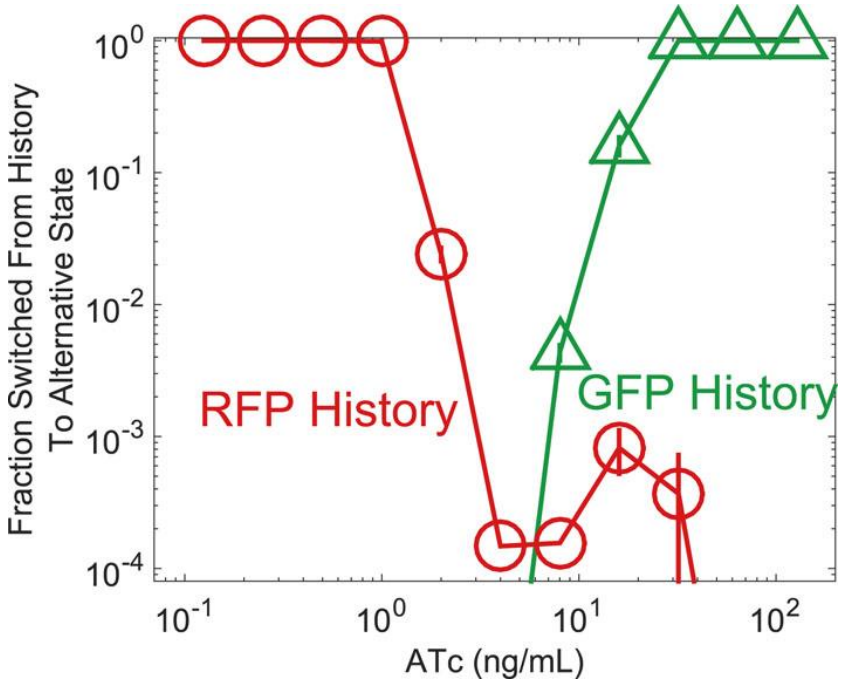

Figure 1.2: Fraction switched after 92 hr of growth, a proxy for the instability of the state, increases approaching a phenotypic switch.

Yeast cells were pre-grown in the GFP state (green triangles) or RFP state (red circles) and then transferred to a range of ATc concentrations. After 92 hr of growth, the fraction of cells that have switched from their history state to the alternative state is plotted vs ATc. Error bars represent the standard error from three different samples of Forward Scatter Area vs Side Scatter Area (FSC-A vs SSC-A). See Figure 1.4 for details of how a gate is drawn.

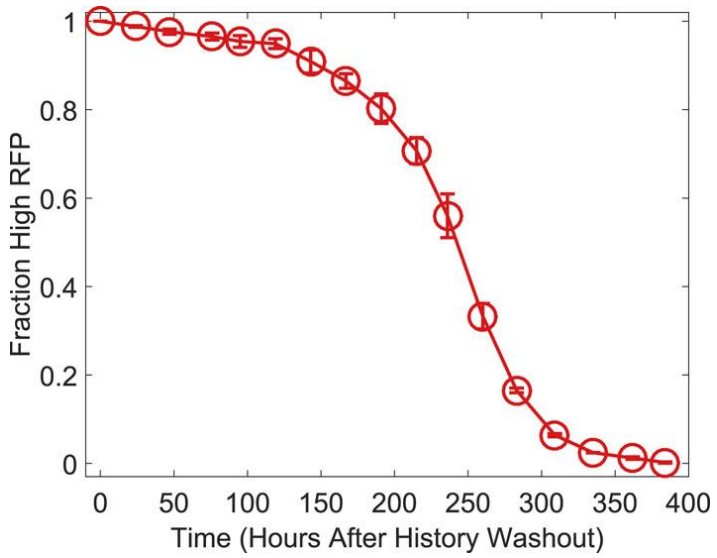

Figure 1.3: The switching kinetics are non-exponential.
Cells were pre-grown in the high RFP state and then transferred to 40 μM IPTG and 2 ng/ml ATc. The fraction of cells remaining in a high RFP state is plotted as a function of time. The switching kinetics are more complicated than what one would expect from first-order kinetics. Error bars represent the standard error from three different samples of FSC-A vs SSC-A.

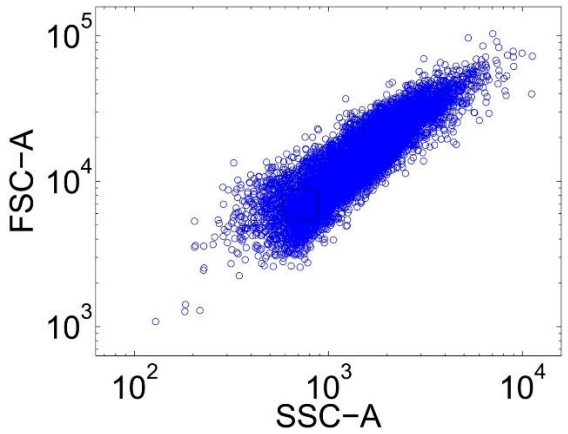

Figure 1.4: To control for cell size, tight gates on FSC-A vs SSC-A are selected for analysis.
10,000 events are collected on the flow cytometer, and the forward scatter area and side scatter area are plotted for each event. A narrow gate (shown in black dashed lines) is drawn to select a subset of cells (approximately 200) for analysis. This effectively decouples fluorescence from cell size, so that differences in fluorescence are due to differences in expression of fluorescent proteins. Error bars in most plots are determined by analyzing three randomly chosen gates and calculating the standard error.

1.2 Resilience to directional perturbations

In analogy to other complex systems, we hypothesized that phenotypic states in this gene network might become increasingly sensitive to perturbations near a critical transition[22]. This expectation arises because the state's basin of attraction shrinks as the stable and unstable fixed points approach one another (Figure 1.5A). Brief environmental perturbations will push the system out of equilibrium. If the system is far from the critical transition it will return to its original state after the perturbation is removed (Figure 1.5B). However, close to the critical transition, the same perturbation might cause the system to cross the basin boundary, thus causing the cell to switch phenotypic states. Therefore, phenotypic states are expected to lose resilience to environmental perturbations near a critical transition.

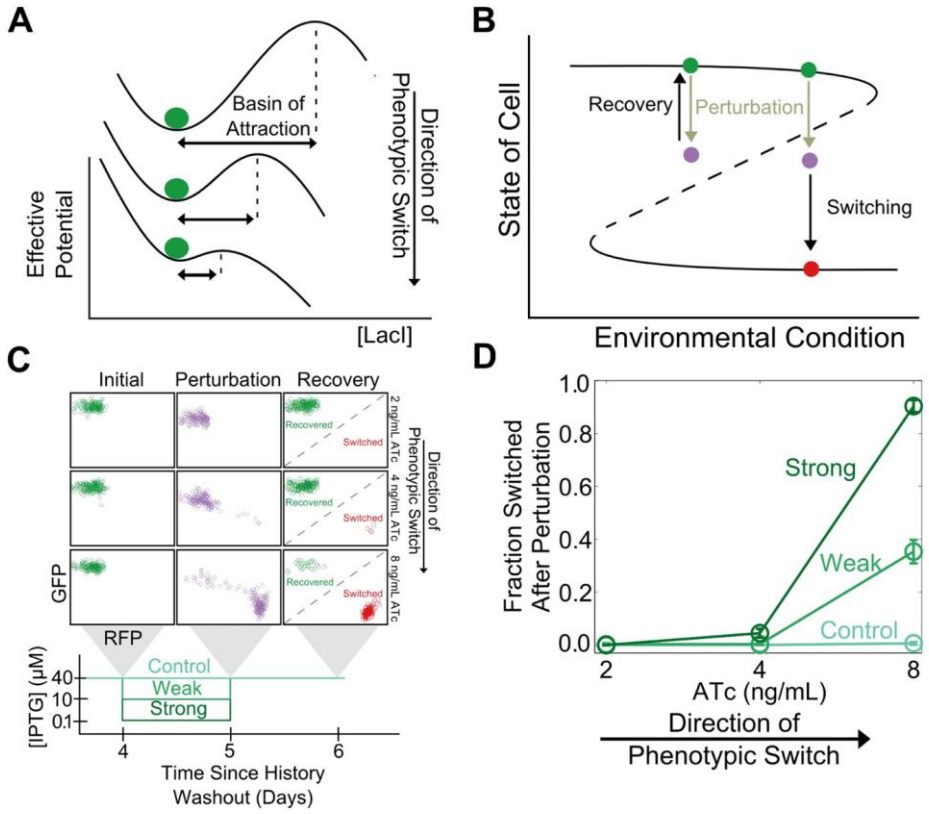

Figure 1.5: resilience of GFP state to directional perturbations

Figure 1.5 (continued): Cellular memory of the high GFP history in the toggle switch loses resilience to directional.

(**A**) A schematic of how the effective potential changes and the basin of attraction shrinks approaching the critical transition. The size of the basin of attraction is determined by the distance between the stable and unstable fixed points. (**B**) Far from the critical transition, a perturbation temporarily depresses the value of GFP; the system recovers to its initial state after the perturbation is removed. Close to the critical transition, the same perturbation causes the system to cross the basin boundary into the alternative state. (**C**) 92 hr after history washout, cells at different distances from the phenotypic switch were exposed to a reduction in (IPTG) from 40 μM to 0.1 μM. Cells grew for 24 hr in this new condition. IPTG was then restored to 40 μM and cells were allowed to recover for 24 hr. Control cells were propagated with (IPTG) held fixed at 40 μM. (**D**) The fraction of cells that switched into a high RFP state in response to the perturbation is plotted as a function of distance from the tipping point. Two different strength perturbations, a weak (10 μM) and a strong (0.1 μM) are plotted. Error bars in **D** represent the standard error of three different samplings from forward scatter area (FSC-A) vs side scatter area (SSC-A) (see Figure 1.4).

To test this theoretically proposed loss of resilience we perturbed cells at different distances from the critical transition (i.e. different ATc concentrations) and measured how likely the cells were to switch into the alternative phenotypic state as a result of environmental perturbations. We examined two classes of perturbations, "directional" (in which the perturbation increased the probability of switching into the alternative state by inhibiting one or another of the two transcription factors that form the toggle switch) and "generic" (in which the interaction between the toggle switch and the perturbation was not immediately obvious).

To explore the directional perturbation we prepared cells in the GFP state by pre-growing them in IPTG. We then transferred the populations to multiple ATc concentrations for four days, leaving the cells in the high GFP state but at varying distances from the critical transition. At the end of the fourth day, the cells were then perturbed by decreasing the concentration of IPTG for one day before returning the IPTG concentration to its original value. Far from the critical

transition (2 ng/mL ATc), the IPTG perturbation caused almost no cells to switch their phenotypic state (Figure 1.5C). However, close to the critical transition (8 ng/mL ATc), the perturbation caused a great majority of the cells to switch into a high RFP state. Even after the perturbation was removed and the initial conditions were restored, many cells remained in a high RFP state. As expected, the severity of the environmental perturbation (i.e. the magnitude of reduction in IPTG) correlated with the fraction of cells that switched states in response to the perturbation (Figure 1.5D). Importantly, there was negligible switching (~ 0.5%) into the high RFP state for control cells grown in constant IPTG concentrations, demonstrating that the phenotypic switching was indeed caused by the perturbation. Moreover, the lack of phenotypic switching in the absence of the perturbation also indicates that in all of these conditions the traditional measure of cellular memory—the lifetime of the state—would classify all of these conditions as being stable with a high degree of cellular memory. Similar results were observed in the other direction, as cells pre-grown in the RFP state approach the critical transition associated with sudden switching to the GFP state (Figure 1.6). Thus, phenotypic states in the toggle switch lose resilience to directional perturbations near a critical transition.

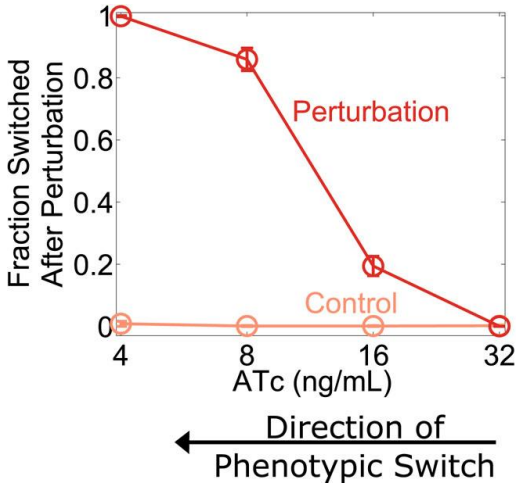

Figure 1.6: resilience of RFP state to directional perturbations

Figure 1.6 (continued): Cellular memory of the high RFP phenotypic state of the toggle switch loses resilience to directional perturbations.
Cells were pre-grown in the RFP state. 92 hr after history washout, cells at different distances from the phenotypic switch were exposed to an increase in (IPTG) from 40 μM to 360 μM. Cells grew for 24 hr in this new condition. IPTG was then restored to 40 μM and cells were allowed to recover for 24 hr. The fraction of cells that switched into a high GFP state in response to the perturbation is plotted as a function of (ATc). Control cells were propagated with (IPTG) held fixed at 40 μM. Error bars represent the standard error of three different samplings from forward scatter area (FSC-A) vs side scatter area (SSC-A).

1.4 Resilience to generic perturbations

Cellular memory in development and cell cycle progression must be resilient against a wide range of different environmental perturbations. Given this, we wanted to explore whether memory in the toggle switch would lose resilience against generic perturbations approaching a critical transition. Cells from a high GFP history at different distances from the phenotypic switch (2, 4, and 8 ng/mL ATc) were perturbed in several different ways for 24 hours: heat stress, osmotic stress with sodium chloride, ethanol stress, and a glucose pulse. Remarkably, we observed a loss of resilience against all four of these generic perturbations (Figure 1.7A, B). Far from the critical transition (2 ng/mL ATc), there was little to no phenotypic switching in response to any of these "generic" perturbations. However, close to the critical transition (8 ng/mL ATc) we observed nearly complete switching in all perturbations, despite the fact that there was essentially no switching (~ 0.5%) in the absence of the perturbations. At a given distance from the phenotypic switch, increasing the strength of a generic perturbation increased the probability that cells would switch into the alternative state (Figure 1.8). The switching induced by the glucose perturbation can perhaps be understood by the fact that glucose shuts down expression of the entire system (LacI, TetR, GFP, and RFP) via catabolite repression of a GAL1 upstream activation sequence, thus pushing the cells toward a low GFP and low RFP

state[18,20]. The other three perturbations have much broader effects on the cell with no obvious connection to the toggle switch network being probed in our experiments. Cellular memory can therefore degrade near a critical transition for a wide range of different environmental perturbations (Figure 1.7C).

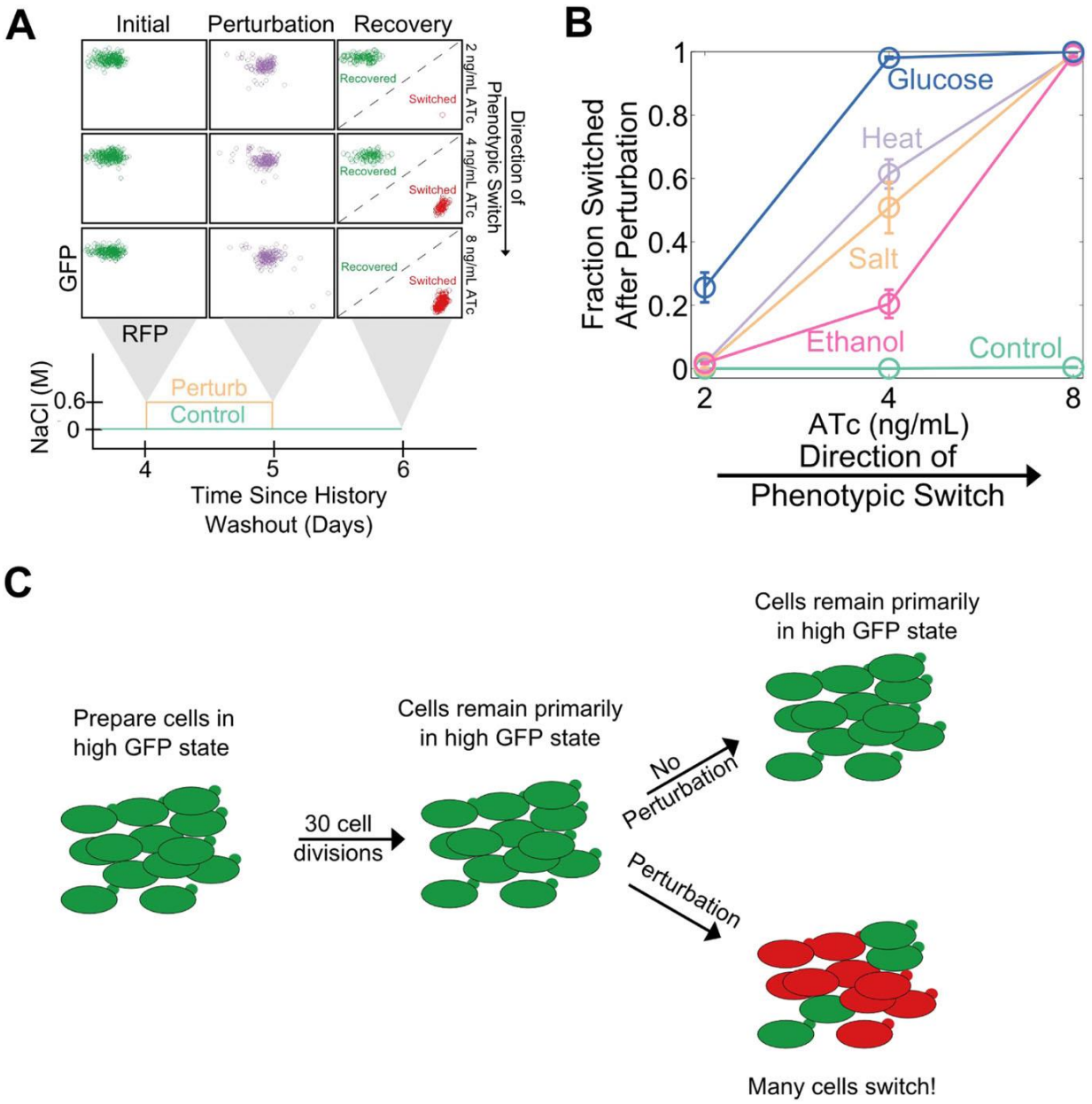

Figure 1.7: Cellular memory of the high GFP history in the toggle switch loses resilience to generic perturbations.

Figure 1.7 (continued): (**A**) Cells were pre-grown in the high GFP state. 92 hr after history washout, cells at 2, 4, and 8 ng/ml ATc were exposed to an osmotic stress (600 mM NaCl). Cells grew for 24 hr in this new condition. The osmotic stress was then removed and cells were allowed to recover for 24 hr. Control cells were propagated with NaCl held constant throughout the whole time course. Growth media contains trace NaCl (2 mM). (**B**) The fraction of cells that switched into a high RFP state is plotted as a function of [ATc]. During the 24 hr perturbation period, cells were exposed to 6% ethanol (pink), 600 mM NaCl (peach), 37°C (violet), 0.2% glucose (blue), or no perturbation (teal). Error bars in **B** represent the standard error of three different samplings from FSC-A vs SSC-A. All results were replicated in a second independent experiment several weeks later (see Figure 1.9). (**C**) A schematic of the key findings from the perturbation experiments.

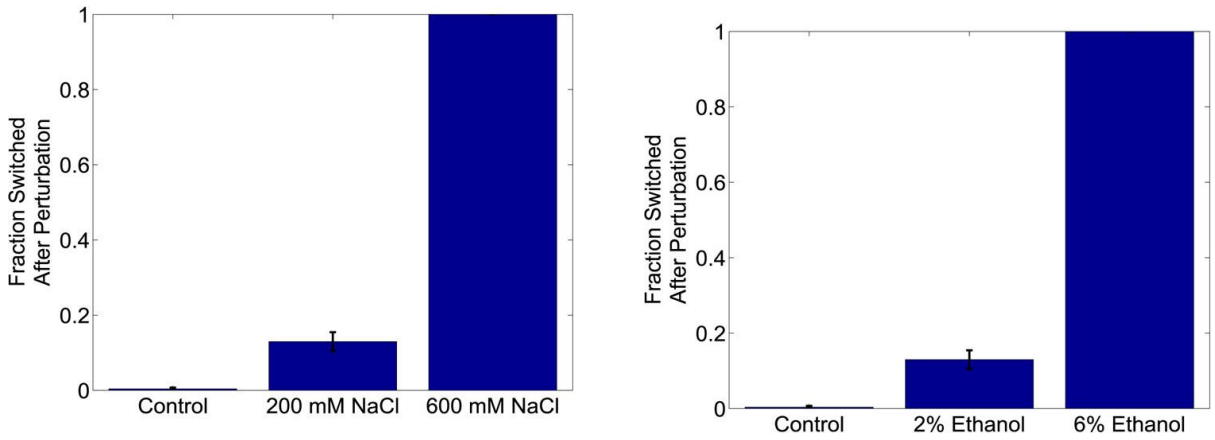

Figure 1.8: Increasing the strength of a generic perturbation increases the probability that cells will switch into the alternative phenotypic state.

Yeast cells expressing the toggle switch were pre-grown in a high GFP state and then transferred to an environmental condition that is close to the phenotypic switch ([ATc] = 8 ng/ml). Cells were perturbed for 24 hr with a salt (left panel) or an ethanol pulse (right panel) and then allowed to recover for 24 hr. The fraction of cells that switch into the high RFP state in response to the perturbation is plotted as a function of perturbation intensity. ATc and IPTG were held fixed throughout the perturbation and recovery periods. Control cells were propagated with no supplemental salt or ethanol for comparison. Error bars represent the standard error of measurements from three different gatings on FSC-A vs SSC-A.

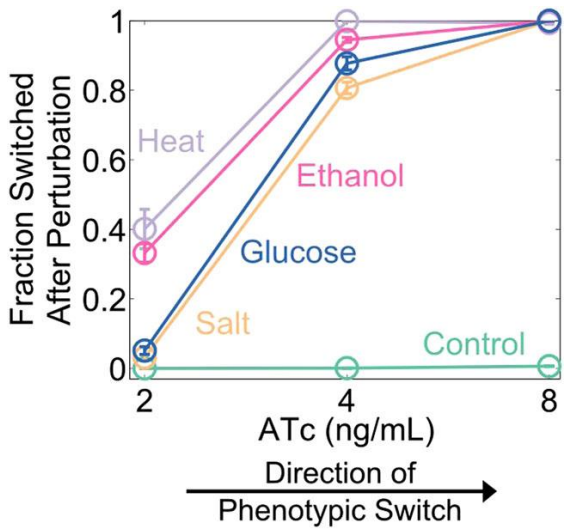

Figure 1.9: A loss of resilience to generic perturbations was confirmed in a second independent experiment.

Same experiment as Figure 1.7B. Yeast cells expressing the toggle switch were pre-grown in the high GFP state and then transferred to different distances from the critical transition (2, 4, or 8 ng/ml ATc). After 92 hr of growth, the cells were perturbed for 24 hr and then allowed to recover for 24 hr. The fraction of cells that switched into a high RFP state is plotted as a function of (ATc). During the perturbation period, cells were exposed to 6% ethanol (yellow), 600 mM NaCl (peach), 37°C (violet), 0.2% glucose (blue), or no perturbation (teal).Error bars represent the standard error of three different samplings from FSC-A vs SSC-A.

Complex dynamic systems near critical transitions are predicted to lose resilience to a specific class of perturbations: those that push the system toward the alternative stable state. However, the effect of a salt shock or a heat shock on the GFP output of the toggle switch is challenging to predict a priori. Notably, it is possible that some generic perturbations will stabilize the state of the cells and reduce their probability of switching. Indeed, we found that none of the four generic perturbations led to a loss of resilience in the transition from the high RFP state (Figure 1.10, left panel). This result is unsurprising given that the perturbations did not strongly push the genetic network toward the high GFP state (Figure 1.10, right panel). For the salt, ethanol, and heat stresses, the perturbation increased the RFP output of the cells, thereby

stabilizing the state. Thus, phenotypic states in the toggle switch only loss resilience to perturbations that push the system toward the alternative state.

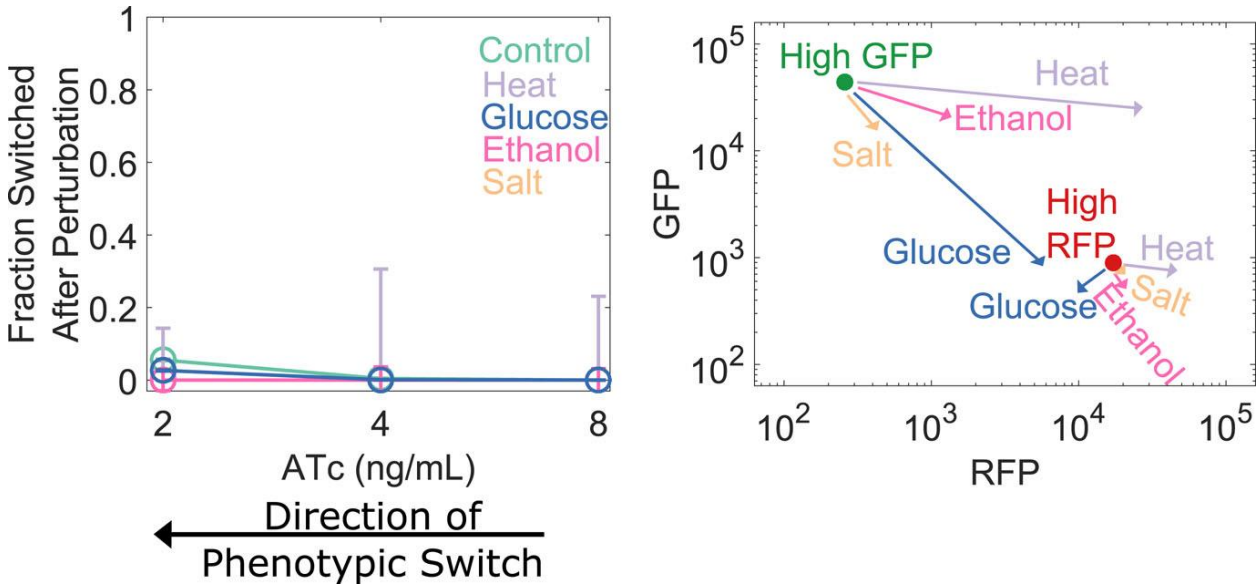

Figure 1.10: Cellular memory of the RFP state of the toggle switch does not lose resilience to generic perturbations because salt, ethanol, and heat shocks stabilize the high RFP state. (Left Panel) Yeast cells were pre-grown in the high RFP state. 92 hr after history washout, cells at 2, 4, and 8 ng/ml ATc were exposed to 6% ethanol (pink), 600 mM NaCl (peach), 37°C (violet), 0.2% glucose (blue), or no perturbation (teal). Cells grew for 24 hr in this new condition. The perturbation was then removed and cells were allowed to recover for 24 hr. Control cells were propagated in 2% galactose and 30°C with no salt or ethanol. The fraction of cells that switched into a high GFP state is plotted as a function of (ATc). (Right Panel) The cells were pre-grown in a high GFP state (green) or high RFP state (red) and then transferred to an intermediate distance from the phenotypic switch (4 ng/ml ATc). 92 hr after history washout, the cells were perturbed as described above. The mean fluorescence shifts from its pre-perturbation location (red or green dot) to the tip of the perturbation arrow. Error bars in the left panel represent the Laplacian-corrected binomial counting error.

1.5 Mapping the bifurcation diagram

We reasoned that our experimentally-observed loss of resilience could be caused by a shrinking basin of attraction of the phenotypic state. To test this hypothesis, we used our

perturbation experiments to estimate the location of the basin boundary in GFP-RFP space and see how it shifted for different concentrations of ATc (Figure 1.11A). For a given concentration of ATc and a chosen perturbation, we measured the fraction of cells that switched into the alternative state at the end of the recovery period. Analysis of the GFP-RFP distribution at the end of the perturbation and before the recovery period revealed that many cells were in an indeterminate state between the two stable phenotypic states. We ranked the cells according to the ratio of GFP expression to RFP expression and assumed that a cell would switch phenotypic states when its ratio of GFP expression to RFP expression fell below a critical threshold. This is equivalent to assuming that the basin boundary between the two phenotypic states takes the form of a line on a log-log plot. To justify this assumption, we used a simple mathematical model of the toggle switch (see Figure 1.12). Our modeling indicated that this assumption would hold as long as the promoter strengths of the two transcription factors in the toggle switch were approximately equal.

Using the assumption described above, we estimated the location of the basin boundary consistent with our experimentally observed fractions at the end of the recovery period. Encouragingly, we find that for a given concentration of ATc, the switching fraction for the eight different perturbations (weak and strong IPTG, weak and strong ethanol, weak and strong salt, heat, glucose) is well fit by a single separatrix (Figure 1.11B). Moreover, as ATc increases from 2 to 8 ng/mL, the location of the basin boundary gets closer to the location of the high GFP stable fixed point (Figure 1.11C). Knowing the location of the basin boundary allowed us to map the bifurcation (Figure 1.11D). Thus, the loss of resilience appears to be driven by a shrinking basin of attraction of the phenotypic state.

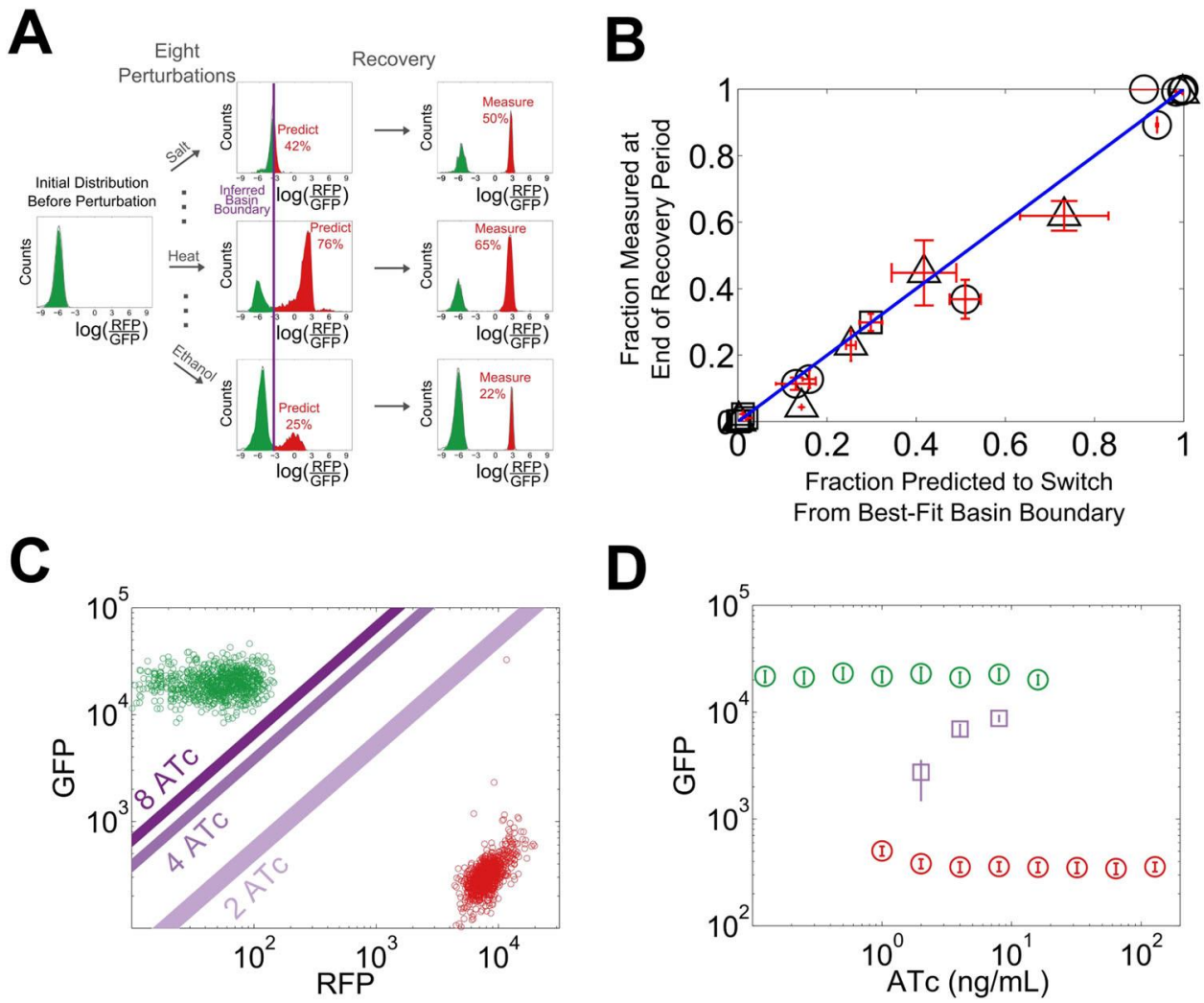

Figure 1.11: The loss of resilience is due to a shrinking basin of attraction of the phenotypic state.

(**A**) By examining the RFP-GFP distribution at the end of the recovery period and comparing it to the end of the perturbation period, the basin boundary can be estimated. A cell is assumed to switch when its ratio of GFP to RFP expression falls below some threshold α, so the separatrix is a line with slope 1 and intercept α on a log–log plot. A simple model of the toggle switch supports this assumption (see Figure 1.12). For each [ATc], eight perturbations (10 μM IPTG, 0.1 μM IPTG, 37°C, 200 mM NaCl, 600 mM NaCl, 2% ethanol, 6% ethanol, and 0.2% glucose) were used to estimate α by minimizing the mean-squared deviation between the estimated and measured fractions. (**B**) The estimated fraction is compared to the measured fraction for [ATc] = 2 ng/ml (□), 4 ng/ml (Δ), and 8 ng/ml (○). (**C**) The unperturbed GFP-RFP distribution for cells at

Figure 1.11 (continued): 0 ng/ml (green) and 128 ng/ml (red) is overlaid with the estimated separatrix from 2, 4, and 8 ng/ml. $\mu \pm \sigma$ is shaded for each separatrix. (**D**) The location of the high GFP stable fixed point (green), unstable fixed point (purple), and low GFP stable fixed point (red) are plotted as a function of ATc. The system is bistable for intermediate ATc and monostable at low and high ATc. We assume that switching follows a line in log-space connecting the centroids of the two distributions in Figure 1.11C (see Figure 1.13). Error bars in all plots represent the standard error from three samplings from the FSC-A vs SSC-A distribution.

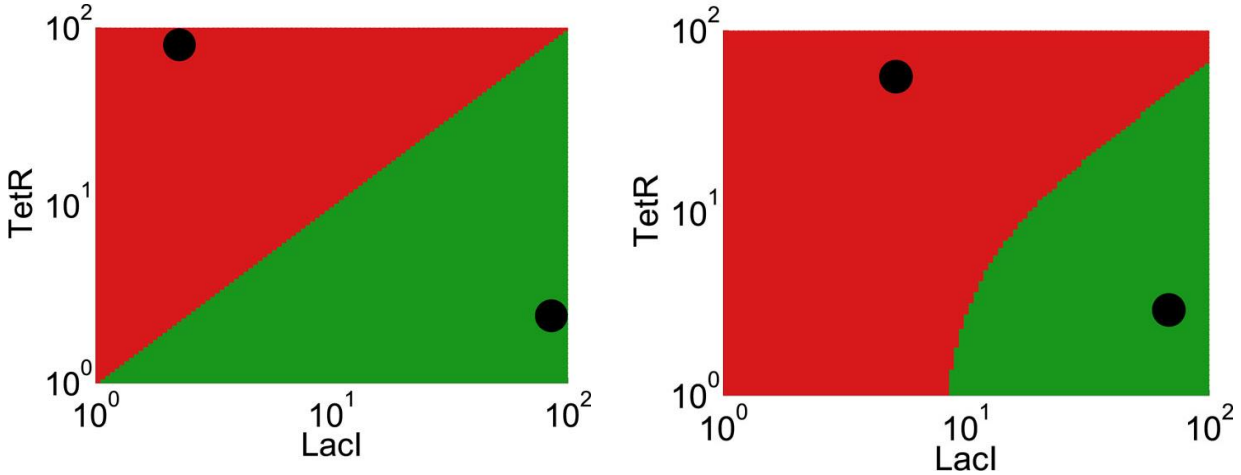

Figure 1.12: A simple model of the toggle switch justifies the assumption that the basin boundary can be approximated as a line in LacI-TetR space.

A deterministic model features cooperative binding of repressor proteins to their promoters (see section 1.9 for further details). The system was initialized with a wide range of initial concentrations of LacI and TetR. The system then evolved in time until it reached one of the two stable fixed points. Initial conditions leading to a high LacI state are shaded in green, and initial conditions leading to a high TetR state are shaded in red. The stable fixed points are represented by black circles. The basin boundary is the interface where the red and the green areas meet. Left: the promoters have equal strengths and right, the promoters have asymmetric strengths. See also the grey line in figure S7 of work by Wu and colleagues[20].

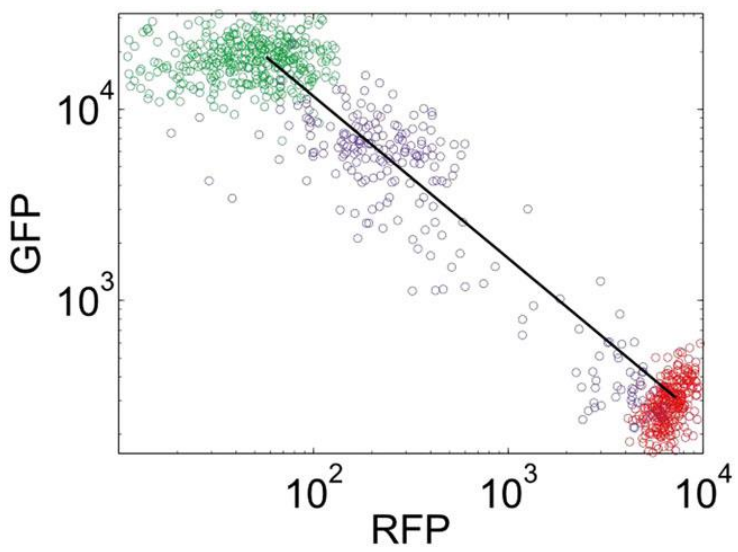

Figure 1.13: Cell switching paths approximately follow a line on a log–log plot connecting the stable fixed points.

Yeast cells in a high GFP condition (2 ng/ml ATc) are plotted in green and cells in a high RFP condition (128 ng/ml ATc) are plotted in red. The line connecting the centroids of the distribution is plotted in black. Overlaid in purple is the distribution of cells that were initially in a high GFP state and were then perturbed for 24 hr with a glucose pulse. The unstable fixed point in Figure 1.11D is estimated by finding the y-coordinate of the intersection of the basin boundary in Figure 1.11C with the black line above.

1.6 Early Warning Indicators of Critical Transition

Given that the phenotypic states associated with our toggle switch lose resilience to perturbations near the critical transition, a natural question is whether, just as in other examples of critical transitions in complex systems such as ecosystem collapse, it is possible to develop warning indicators that this loss of resilience is taking place[16]. For example, one might expect that the mean GFP of cells in the high GFP state would decrease with increasing ATc, thus potentially signaling that the critical transition is approaching[23]. However, we find that the mean GFP of unswitched cells is approximately constant over the range of ATc concentrations in which we observe a loss of resilience (Figure 1.1B and Fig. 1.14A). Researchers in a number of

fields have explored early warning indicators based on a loss of stability near a critical transition (broadening of the effective potential as illustrated in Figure 1.5A)[17]. This loss of stability would manifest in our experiments as an increase in the variation of GFP fluorescence among the population of (unswitched) cells. However, we find experimentally that there is no increase in variation within the population approaching the critical transition, even very close to the transition where the GFP state is metastable (Figure 1.14B and C). The theoretically proposed early warning indicators based on local stability therefore fail to predict the critical transition in this gene network[24].

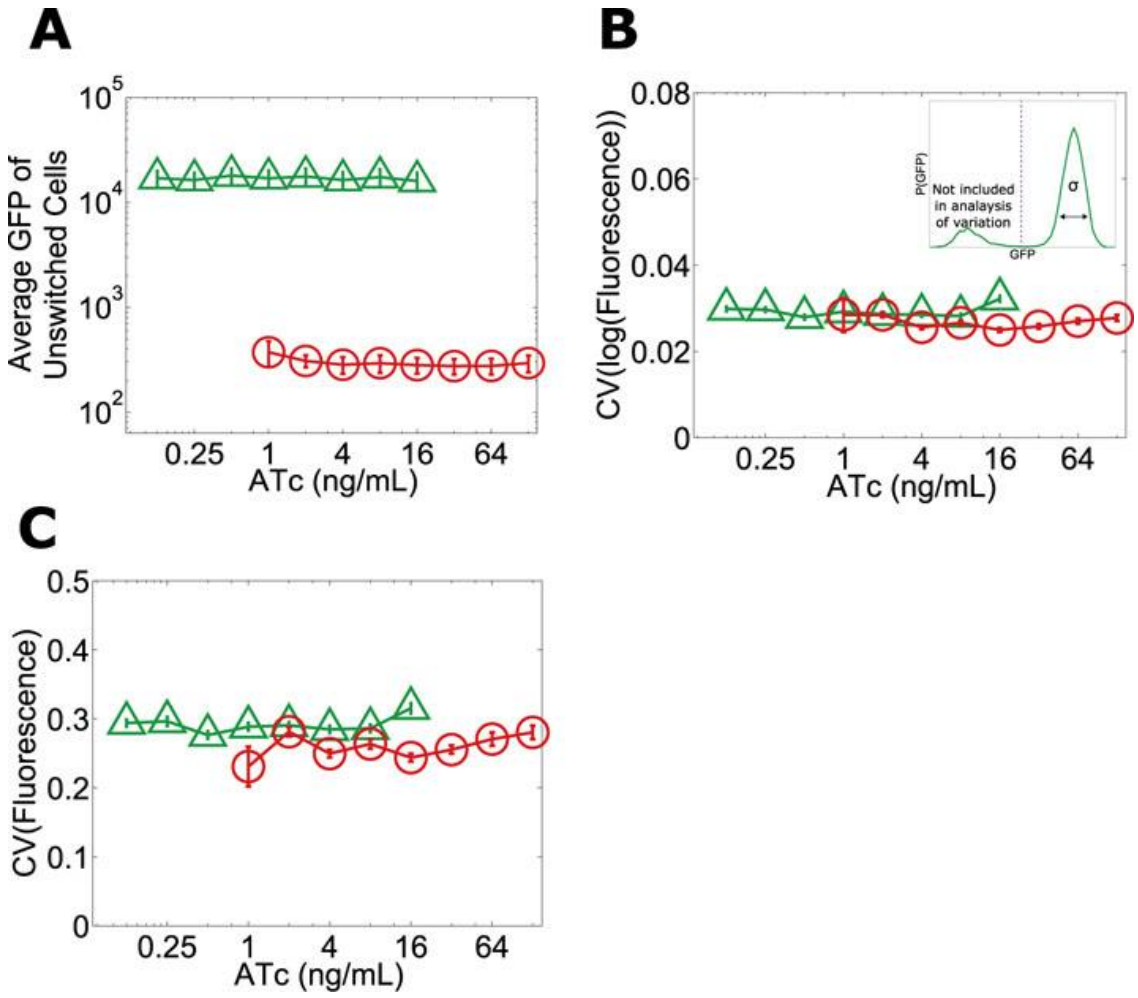

Figure 1.14: early warning indicators of impending bifurcation

Figure 1.14 (continued): No significant change in mean fluorescence of the state and no significant increase in coefficient of variation approaching the critical transition.
Yeast cells expressing the toggle switch were pre-grown in the high GFP state (green triangles) or the high RFP state (red circles) and then transferred to a range of ATc concentrations for 92 hr. (**A**) The mean GFP fluorescence of cells that have not switched from their pre-growth state is plotted against [ATc]. Above 16 ng/ml (for the GFP history) and below 1 ng/ml (for the RFP history), all of the cells have switched into the alternative state. To quantify population variability, the standard deviation normalized to the mean (coefficient of variation, i.e., 'CV') is plotted for the **B**, log-transformed and **C**, linear values of fluorescence. When calculating variation, only cells that remain in the state they were pre-grown in are analyzed (see inset in **B**). To minimize the effect of instrument noise in **B** and **C**, variation in RFP fluorescence is measured for the RFP history (similarly, variation in GFP is measured for the GFP history). Error bars in **A** represent the standard error of three samplings from FSC-A vs SSC-A. Error bars in **B** and **C** are standard errors from 200 bootstrap resamplings of the data.

1.7 Yeast GAL and *E Coli* Lactose Network Experiments

To explore the generality of our results, we chose to study the yeast GAL network, which displays an "all-or-none" response in some sugar environments containing galactose[25,26]. However, the wild-type GAL network exhibits only weak memory[26]. To expand the range of galactose concentrations for which the system has memory[4], we used a strain of yeast constitutively expressing the repressor GAL80 (which codes for a transcriptional repressor involved in one of the many feedback loops that stabilize memory in this network). To assess the state of the network, yellow fluorescent protein (YFP) expression was driven by a GAL1 promoter. Cells were pre-grown in high galactose (GAL ON) and then grown for a day in a range of galactose concentrations (Figure 1.15A). We then examined the resilience of the GAL network to perturbations at different distances from its critical transition, similar to our experiments with the toggle switch. For the GAL network, a glucose pulse served as a directional

perturbation (due to catabolite repression[27]), and we again used heat, salt, and ethanol as generic perturbations.

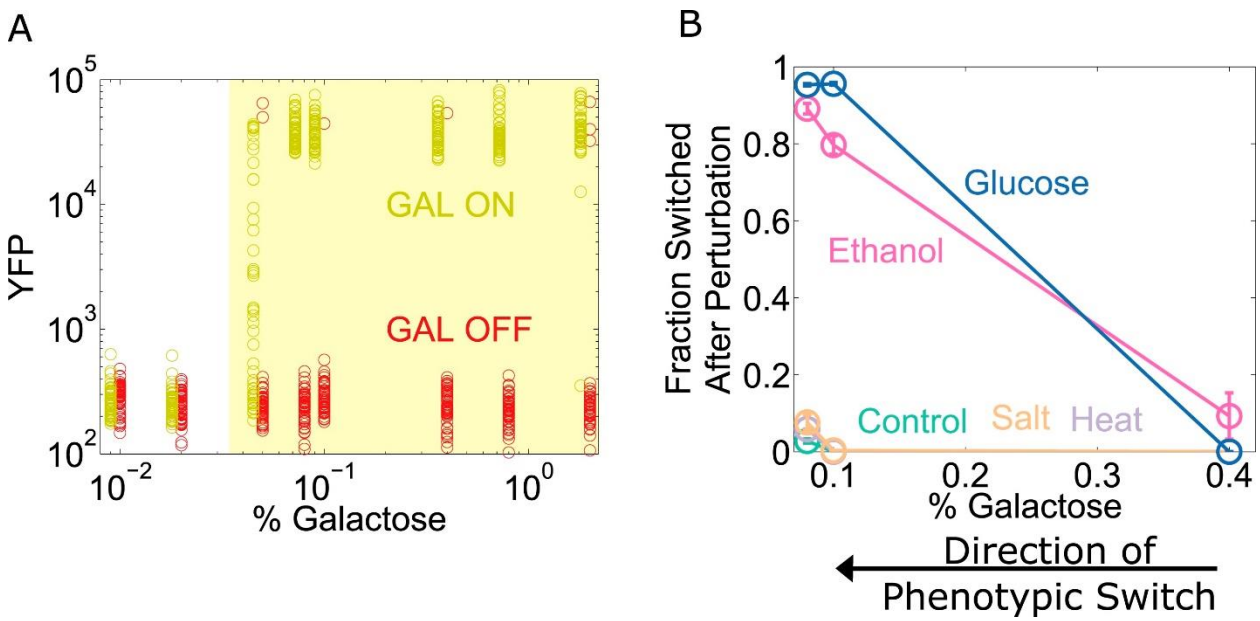

Figure 1.15: The yeast galactose network loses resilience to directional perturbations and the generic perturbation ethanol.
(**A**) 25 hr after history washout, a gal80-inducible strain shows strong memory above 0.05% galactose. The two histories are offset for ease of viewing, and the region of memory is shaded in yellow. 50 cells at random are plotted from a tight gate on FSC-A vs SSC-A. (**B**) 25 hr after history washout, cells at 0.4%, 0.1%, and 0.08% galactose were exposed to 6% ethanol (pink), 600 mM NaCl (peach), 37°C (violet), 0.1% glucose (blue), or no perturbation (teal). Cells grew for 12 hr in this new condition. The perturbation was then removed and cells were allowed to recover for 12 hr. Control cells were propagated with fixed glucose, galactose, and temperature. The fraction of cells that switched into a low YFP state after the perturbation is plotted as a function of [galactose]. Error bars are standard errors obtained by bootstrap with 200 resamplings of the data.

We found that the "GAL ON" phenotypic state lost resilience to glucose and ethanol perturbations but not salt or heat (Figure 1.15B). Similarly, we performed experiments probing the resilience of the ON state in the *E. coli* lac operon, where we again observed a loss of resilience to both directional perturbations and to the generic perturbation ethanol (Figure 1.16).

These three genetic switches have widely different architectures, and operate in two different species. Our results thus indicate that a loss of resilience approaching a phenotypic switch could be a general property of multistable gene networks and that "generic" or global perturbations, such as temperature or salt shocks, can cause widespread loss of cellular memory.

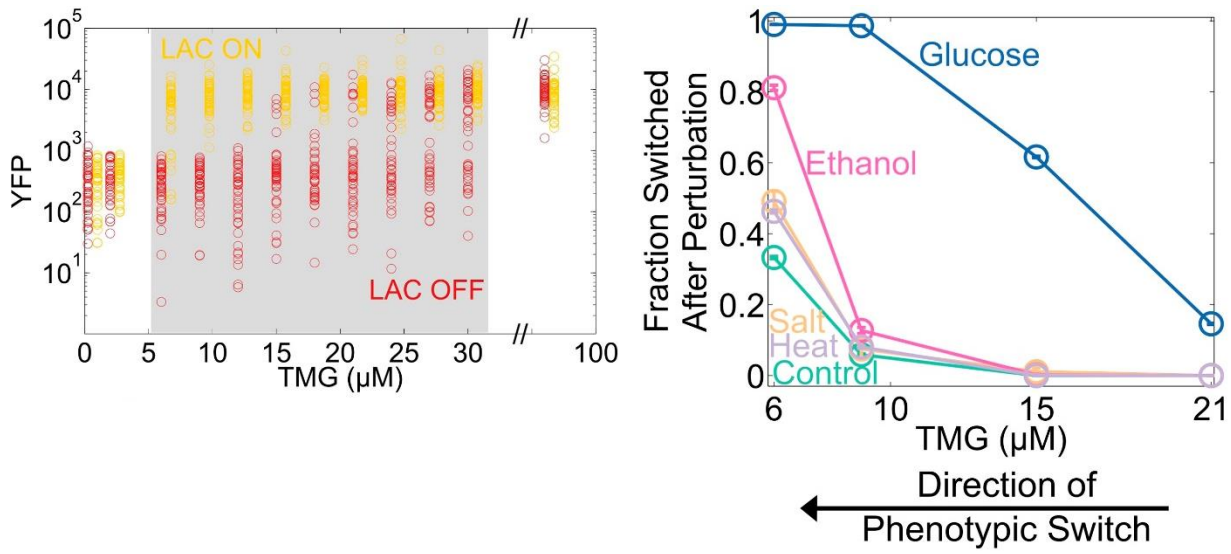

Figure 1.16: The *Escherichia coli* lactose network loses resilience to directional perturbations as well as to the generic perturbation ethanol.
(Left panel) The cells were pre-grown in either 0 or 100 μM TMG ('LAC OFF' and 'LAC ON,' respectively) for 20 hr and then diluted into a range of TMG concentrations. After 21 hr of growth, the system exhibits strong hysteresis. A constitutively expressed mCherry allows for discrimination between OFF cells and noise. The region of memory is shaded in gray, and the two histories are offset for ease of viewing. Fifty cells at random are plotted. (Lower panel) 21 hr after pre-growth washout, the cells from the ON history were exposed to several perturbations for 12 hr (blue: 0.01% glucose; pink: 6% ethanol; peach: 1 M NaCl; violet: 43°C). The perturbations were then removed, and the cells were allowed to recover for 12 hr. The fraction of cells that switched into the OFF state is plotted as a function of [TMG]. Control cells (green) were grown at 37°C with no added salt, glucose, or ethanol. Error bars represent the standard error from 200 bootstrap resamplings of the data.

1.8 Discussion

Here we have shown that brief perturbations in the extracellular environment can dramatically increase the rate of phenotypic switching from a highly stable memory state into an alternative state. We argue that this loss of resilience to perturbations near the bifurcation can be explained by a shrinking of the basin of attraction of the phenotypic state. By observing the GFP-RFP distribution at the end of the perturbation period and applying a simple threshold, we were able to accurately predict the fraction of cells that would return to the pre-perturbation memory state at the end of the recovery period. At a given distance from the bifurcation, the same basin boundary was able to accurately predict the switching fraction in response to eight different perturbations. The predictive success of this threshold is particularly impressive given that the different perturbations have dramatically different effects on the GFP-RFP distribution (see Figure 1.11A).

There is an interesting question of the precise mechanism by which the perturbations act on the system to push the cells to a new location in GFP-RFP space. Part of the answer is certainly that the perturbations cause a shift in the stability landscape underlying the phenotypic states. It is also possible that the perturbations cause an increase in noisy gene expression. Understanding what is occurring during the perturbation period, both biochemically and from a dynamical systems perspective, will be an area of investigation for future research.

The perturbations (salt stress, heat stress, etc.) lasted for a significant duration: 24 hr, or roughly 3 to 8 cell divisions. It is interesting to ask whether we would have seen similar results if we had perturbed the system for a shorter duration. To address this question, we performed Gillespie simulations using a very simple phenomenological model of the toggle switch (see section 1.9 for additional details)[28]. Similar to our test tube experiments, we initialized the

system in a high Lac state. The system was allowed to equilibrate for several generations, before we suddenly changed one of the parameters of the system (either the disassociation constant between the transcription factor and the DNA or the promoter strength). We performed this perturbation for a variable duration ranging from 0.2 generations to 20 generations. The system was then allowed to recover (by restoring the parameter to its initial value) for several generations, and we then determined what fraction of cells remained in a high Lac state. Two key observations emerged. (1) The degree of switching is set by both the intensity and duration of the perturbation. For dramatic perturbations, the minimum duration of perturbation to induce switching is approximately set by the cell division time (Figure 1.17). (2) Not all perturbations induced phenotypic switching. Of note, perturbations which stabilized the high Lac state induced negligible switching into the high Tet state (Figure 1.18). These observations held regardless of whether the perturbation was achieved by changing the disassociation constant or the promoter strength.

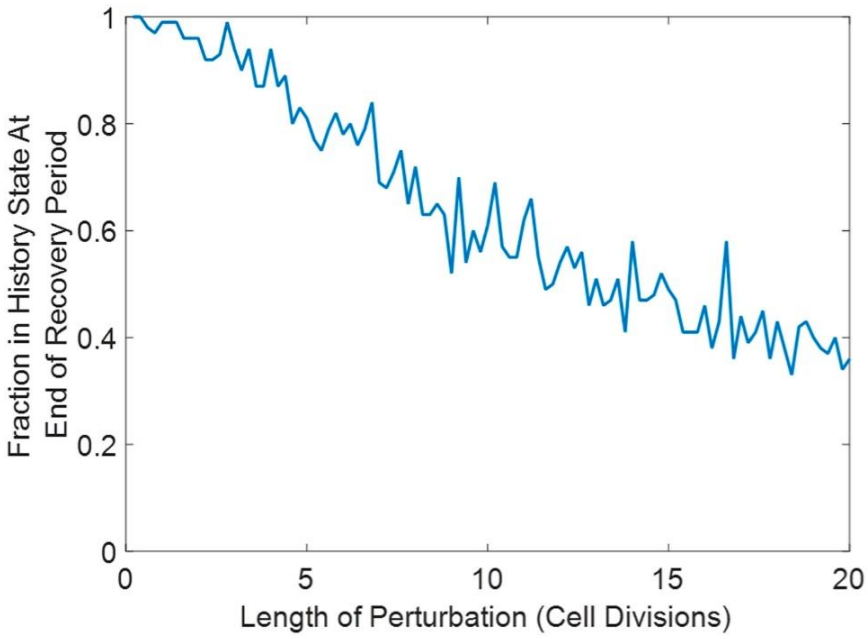

Figure 1.17: Increasing the duration of the perturbation increases the fraction of cells that switch phenotypes in a Gillespie simulation of the toggle switch.

Figure 1.17 (continued): Here, p = 50, K = 15, and γ = 0.5. 100 cells are initialized in a high Lac state and equilibrate for ten generations. Suddenly, K is increased to 100 for a variable time period (ranging from 0.2 to 20 generations). K is then restored to 15, and the cells are allowed to equilibrate for several more generations. At the end of the recovery, we determine what fraction of the cells remains in a high Lac state.

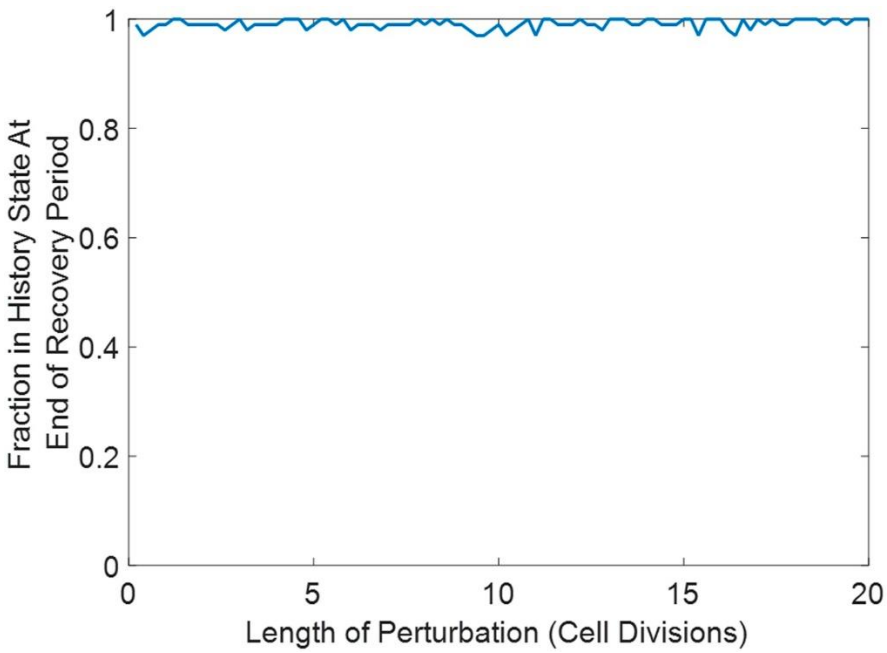

Figure 1.18: Not all perturbations induce switching in a Gillespie simulation of the toggle switch.

Here, p = 50, K = 15, and γ = 0.5. 100 cells are initialized in a high Lac state and equilibrate for ten generations. Suddenly, K is decreased to 1 for a variable time period (ranging from 0.2 to 20 generations). K is then restored to 15, and the cells equilibrate for several more generations. At the end of the recovery, we determine what fraction of the cells remains in a high Lac state.

Understanding the stability of phenotypic states in gene networks remains an important challenge in biology. Here we have demonstrated that for robust cellular memory in natural contexts subject to environmental noise, low rates of stochastic switching from the phenotypic state is not sufficient. This is because the cellular memory must also be robust against environmental fluctuations and perturbations that are impossible to avoid. Here we found

experimentally that several phenotypic states lost resilience to multiple environmental perturbations near a critical transition. Given that over time there will often be multiple kinds of environmental fluctuations and perturbations, our results argue that many forms of cellular memory will become destabilized near a critical transition. Our results provide a roadmap for exploring cellular memory and phenotypic switching in other contexts, from development to cancer progression.

1.9 Appendix: Experimental Methods and Computational Simulations

Strains

Toggle switch strains have been previously characterized[18,20]. Gal80-inducible strains have been previously described[22]. LacY-YFP fusion strains have been previously described[29].

Toggle Switch Experiments

Cells were grown in synthetic media (YNB and CSM – Trp – Leu; Sunrise Science) containing 2% galactose and ATc/IPTG as described in the text. Cells were grown in 3 mL cultures in 14 mL VWR culture tubes and diluted daily to prevent saturation. Cells were pre-grown for 24 hours in either 1 mM IPTG or 250 ng/mL ATc and then transferred to a range of ATc concentrations as described in the text. 20 μL of cells were harvested daily at OD 0.5, diluted in 180 μL PBS, and run immediately on a Miltenyi MACSQuant VYB flow cytometer. After 4 days of serial transfer, cells were transferred to the perturbation environment. Cells grew for 24 hours in this environment before being characterized via flow cytometry and diluted into the original environment they were in before the perturbation (hereafter, the "recovery environment"). Cells grew for 24 hours in the recovery environment and then were characterized with flow cytometry. The basin boundary was estimated by assuming that cells

switched phenotypes when the ratio of GFP to RFP expression fell below a critical threshold. All results were verified in two independent experiments carried out several weeks apart.

GAL network experiments

Cells were pre-grown for 24 hours in either 0.5% galactose or 0.01% glucose (GAL ON and GAL OFF, respectively) plus 0.05 μg/mL doxycycline. Cells were then diluted into 0.01% glucose, 0.05 μg/mL doxycycline, and galactose concentrations ranging from 0 to 2%. Cells were diluted every 12 hours and the OD was kept below 0.01 to minimize consumption of the sugars. Cells were harvested every 12 hours, concentrated via centrifugation, and characterized immediately via flow cytometry. Cells were transferred to the perturbation environment 24 hours after history removal. They were then grown for 12 hours, characterized via flow cytometry and diluted into the recovery environment, grown for a further 12 hours, and characterized via flow cytometry.

Lac network experiments

Cells were grown in M9 media with .1% succinic acid as a carbon source. Cells were first pre-grown in either 0 or 100 μM TMG ("Lac OFF" and "Lac ON," respectively) for 20 hours. The history condition was then washed out, and the two populations were then separately transferred to a range of TMG concentrations. Cells grew for 21 hours. YFP expression was assayed using flow cytometry as a proxy for the state of the Lac network. A constitutively expressed RFP enabled for discrimination between cells and noise. 21 hours after history washout, cells were diluted into the perturbation environment and grown for 12 hours. After 12 hours of growth, YFP expression was again assayed using flow cytometry. At the same time, the cells were diluted into the recovery environment and grown for a further 12 hours. At the end of the recovery period, YFP expression was again assayed using flow cytometry.

Data Analysis

Flow cytometry data was analyzed utilizing the Gore lab's flow cytometry tool kit, which can be accessed at http://gorelab.bitbucket.org/flowcytometrytools/.

Theoretical Model for the Toggle Switch

The rate of production of the two repressors is described by the following equations:

$$(1) \quad [\dot{LacI}] = \frac{P_{Tet}}{1 + \left(\frac{[TetR]}{K_{Tet}}\right)^2} - \gamma[LacI]$$

$$(2) [\dot{TetR}] = \frac{P_{Lac}}{1 + \left(\frac{[LacI]}{K_{Lac}}\right)^2} - \gamma[TetR]$$

The promoter strength is determined by the DNA sequence and has been previously characterized[18]. As a simple approximation, we treat ATc and IPTG as modulating K_{Tet} and K_{Lac}. We assume that the proteins are stable, so the rate of transcription factor degradation is set by dilution via cell division.

Our primary goal for the model was to predict the shape of the basin boundary between the two phenotypic states, particularly in a system where the promoter strengths are asymmetric. Figure 1.12 was generated by picking values of K_{Tet} and K_{Lac} so that the system exhibited bistability over a range of [LacI] and [TetR]. We initialized the system with many different [LacI] and [Tet] and allowed the system to evolve according to equations 1 and 2 until the system reached a steady state.

For the equal promoter strengths, the following parameters were used:

$P_{Lac}=P_{Tet}=50$
$K_{Lac}=K_{Tet}=15$
$\gamma_{Lac}=\gamma_{Tet}=0.5$

For the unequal promoter strengths, the following parameters were used:

P_{Lac}= 30
P_{Tet}=35
K_{Lac}=K_{Tet}=15
γ_{Lac}=γ_{Tet}=0.5

For the Gillespie simulations to investigate the effect of perturbation duration on switching fraction, we again used:

P_{Lac}=P_{Tet}=50
K_{Lac}=K_{Tet}=15
γ_{Lac}=γ_{Tet}=0.5

Similar to our test tube experiments, we initialized the system in a high Lac state. The system was allowed to equilibrate for several generations, before we suddenly changed one of the parameters of the system (either the disassociation constant between the transcription factor and the DNA or the promoter strength). We performed this perturbation for a variable duration ranging from .2 generations to 20 generations. The system was then allowed to recover (by restoring the parameter to its initial value) for several generations, and we then determined what fraction of cells remained in a high Lac state.

Chapter 2

Yeast Cross-feeding Mutualism Dynamics

Mutualisms between species play an important role in ecosystem function and stability. However, in some environments the competitive aspects of an interaction may dominate the mutualistic aspects. Although these transitions could have far-reaching implications, it has been difficult to study the causes and consequences of this mutualistic-competitive transition in experimentally tractable systems. Here we study a microbial cross-feeding mutualism in which each yeast strain supplies an essential amino acid for its partner strain. We find that, depending upon the amount of freely available amino acid in the environment, this pair of strains can exhibit an obligatory mutualism, facultative mutualism, competition, parasitism, competitive exclusion, or failed mutualism leading to extinction of the population. A simple model capturing the essential features of this interaction explains how resource availability modulates the interaction and predicts that changes in the dynamics of the mutualism in deteriorating environments can provide advance warning that collapse of the mutualism is imminent. We confirm this prediction experimentally by showing that, in the high-nutrient competitive regime, the strains rapidly reach a common carrying capacity before slowly reaching the equilibrium ratio between the strains. However, in the low-nutrient regime, before collapse of the obligate mutualism, we find that the ratio rapidly reaches its equilibrium and it is the total abundance that is slow to reach equilibrium. Our results provide a general framework for how mutualisms may transition between qualitatively different regimes of interaction in response to changes in nutrient availability in the environment.

2.1 Background and Motivation

Species in a community interact in a bewildering variety of ways, from parasitic to competitive to mutualistic. Mutualisms, in which two species engage in reciprocal cooperative behavior that benefits both partners, are thought to be particularly important for the stability of ecosystems[30,31]. Mutualisms in nature are common and diverse, including the pollination of crops and other plants by bees[32], the cross-protection between clown fish and anemone[33], and the symbiosis between tubeworms and bacteria[34]. In the case of the tubeworm the interaction is completely obligatory, since it has no digestive system and acquisition of energy depends completely on bacterial symbionts. The mutualism between most plants and their pollinators, however, is typically facultative as most plants have multiple pollinators and most pollinators feed from multiple plant species. Despite the fact that species in a mutualism are often referred to as being in an obligate or facultative mutualism, a major focus of recent research on mutualisms has attempted to elucidate the conditions in which a mutualism can break down or switch to a parasitism[35,36]. For example, the cross-protection mutualism between ants and the plants that house them can break down when grazing pressure on the plant is reduced[37].

In many microbial mutualisms, partners benefit from each other through cross-feeding, in which each species supplies their partner with nutrients. Such interactions can be present within a species[38], between pairs of species[39,40] or could represent a complicated network of dependencies[41], and possibly play a major role in driving the diversity of microbial communities in environments such as the soil[42]. Laboratory experiments on microbial ecosystems enable fine-grained control of microbial populations and their environment, providing the potential to integrate experiments and models in ways not possible in the field. Laboratory experiments have been used to show a stabilizing effect of mutualistic interactions on relative abundance of two microbial species[39], which also protected populations against invasion by cheater strains[43].

Recent work demonstrated that novel mutualisms could be established in a variety of circumstances[44,45]. However, these and other laboratory studies generally focused on a narrow range of conditions that result in obligate mutualisms[39,43,44,46]. Therefore, they did not explore how mutualisms are affected when the driving forces behind cooperative interactions are changing, and how this could result in a transition from mutualistic to competitive or other interactions.

In our work, we use a synthetic cross-feeding yeast system in which we modulate the dependence on the mutualism by supplementing the media with the amino acids they cross-feed. By changing these two nutrient concentrations, we are able to switch between a surprisingly large number of different interaction types, including obligatory and facultative mutualism, competition, parasitism and competitive exclusion. Each of these regimes shows qualitatively different dynamics which we can understand using a simple model. Our experiments shed light on the previously underexplored question of how resource availability can modulate the type of interactions between species in a mutualism.

2.2 Synthetic Obligatory Mutualism in Batch Culture

As a model system for mutualistic interactions, we used two non-mating *Saccharomyces cerevisiae* strains that are each unable to produce an essential amino acid yet over-produce the amino acid required by its partner (Figure 2.1A)[40]. The RFP-tagged, leucine auxotrophic strain (Leu^-) overproduces tryptophan, while the YFP-tagged tryptophan auxotroph (Trp^-) overproduces leucine. These strains have previously been demonstrated to form a cross-feeding mutualism when grown on solid agar, with each strain leaking out the amino acid needed by its partner[40].

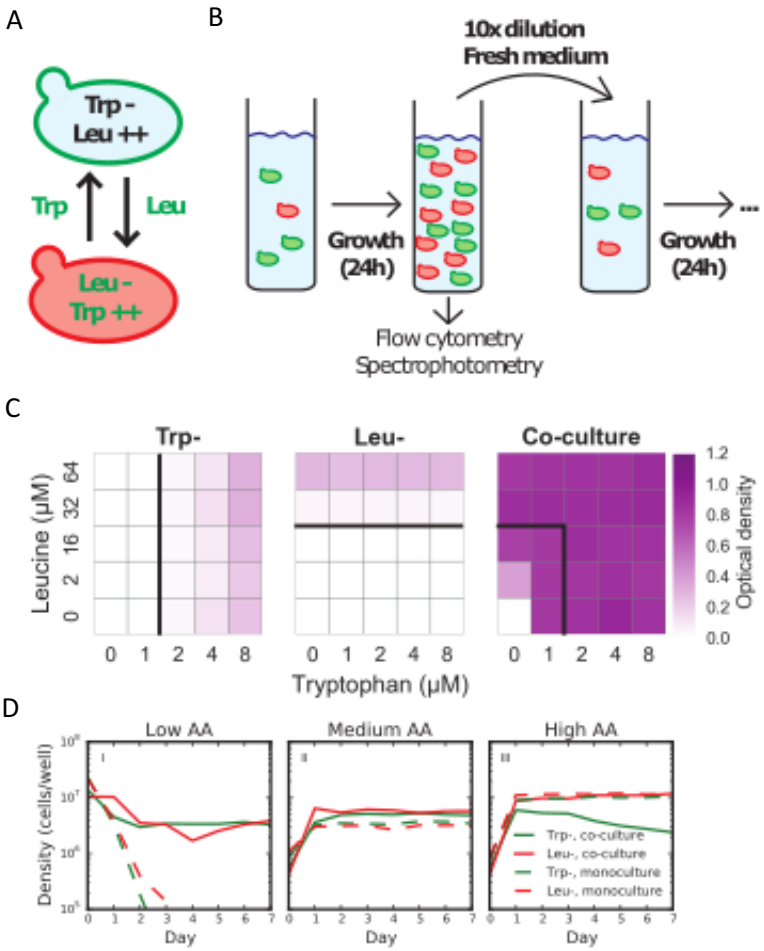

Figure 2.1: Two auxotrophic yeast strains can form a stable cross-feeding mutualism in a range of nutrient concentrations. (A) The YFP-tagged strain is unable to produce the amino acid tryptophan but overproduces the amino acid leucine, whereas the RFP-tagged strain is unable to produce leucine but overproduces tryptophan. (B) The mutualism is probed by co-culturing the two auxotrophic yeast strains in batch culture with 10x dilution daily. Flow cytometry and spectrophotometry report on the relative fraction and total abundance of the two yeast strains at the end of each day of growth. (C) Optical density after eight days of daily dilution and growth. The co-culture is able to survive in low amino acid concentrations where the monocultures cannot survive (solid lines indicate the concentrations below which each auxotrophic strain goes extinct). (D) Abundance of the co-culture (solid line) and monocultures (dashed line) for the Trp- (green) and Leu- (red) strains. In low amino acid concentrations (1 & 8 μM) the strains form an obligate mutualism, in medium amino acid concentrations (8 & 64 μM) the strains form a facultative mutualism, and in high amino acid concentrations (32 & 256 μM) the strains form an amensalism, as the Leu$^-$ strain is relatively unaffected and the Trp$^-$ strain is harmed by the interaction.

To determine if we could establish a stable mutualism between these strains in well-mixed liquid batch culture, we inoculated monocultures and co-cultures at a range of leucine and tryptophan concentrations (Fig 2.1B,C). Co-cultures were started with equal amounts of each strain, at the same total density as monocultures. Each day we diluted by a factor 10 into fresh media containing the same defined concentrations of leucine and tryptophan (Figure 2.1B); survival of the culture over repeated cycles of growth and dilution therefore requires that the population is able to divide at least $\log_2(10) \sim 3.3$ times each day. In monoculture, Trp^- cells required at least 2 μM tryptophan to avoid going extinct due to dilution, while Leu^- cells required a minimum of 32 μM Leucine. In contrast, co-cultures could survive on concentrations of leucine and tryptophan where the monocultures would each go extinct. Co-cultures survived eight of these growth-dilution cycles, indicating a stable mutualism. Even in concentrations where monocultures survived, we found that co-culture density was often much higher than the sum of monoculture densities (Fig 2.1C), suggesting that in this regime the strains were interacting in a facultative mutualism.

Understanding the relative benefits that each partner in the mutualism does or does not receive requires that we also determine the population abundance of each strain at different amino acid concentrations. We therefore co-cultured the strains and measured the population composition by flow cytometry at the end of each day. We tried to make both strains receive equal benefits from the amino acids being supplemented by adding leucine and tryptophan in a ratio of 8 to 1, which is approximately the intracellular ratio of these amino acids[47]. We found that at low amino acid concentrations (1 μM tryptophan, 8 μM leucine; 1 & 8 μM) the strains indeed form an obligate mutualism with an apparently stable coexistence, since relative abundance changes little over time (Fig 2.1D). At medium amino acid concentrations (8 & 64

μM) the strains form a facultative mutualism, with both strains benefiting from the presence of the other strain, yet also surviving when grown in monoculture. At high amino acid concentrations (32 & 256 μM), we observed coexistence of the two strains, but with the Trp^- strain at an equilibrium abundance below what it would have reached in a monoculture. At this high amino acid concentration we therefore found that the strains are forming an amensalism, in which the Leu^- strain is relatively unaffected by the interaction but the Trp^- strain performs worse in coculture than in monoculture. This demonstrates that a simple microbial cross-feeding mutualism can transition into a qualitatively different interaction by a simple change in environmental conditions.

2.3 Phenomenological Model of Mutualism

To gain insight into the transition between the different regimes of interaction in our cross-feeding strains, we implemented a simple phenomenological model designed to capture the essential elements of the interactions between the strains. We assumed that the two strains Trp^- (X) and Leu^- (Y) have a per capita growth rate that is modulated by the mutualistic partner as well as the supplemented amino acids:

$$\frac{dX}{dt} = r_x X \left(\frac{Y+a}{Y+a+\kappa}\right)(1 - X - Y) - \delta X \qquad [1]$$

$$\frac{dY}{dt} = r_y Y \left(\frac{\beta X+a}{\beta X+a+\kappa}\right)(1 - X - Y) - \delta Y \qquad [2]$$

The growth rate of each strain increases with the abundance of the mutualist partner and the needed amino acid, but this benefit saturates via a Michaelis-Menten form. We assume that the supplemented amino acids are always added at a fixed ratio, so we use a single variable 'a' to capture the amount of supplemented amino acids (despite the fact that the two strains are actually consuming different amino acids). Since the 1-to-8 ratio of tryptophan to leucine should give

about equal 'relative' amounts of amino acids, we used the same scaling constant (kappa = 0.12) for both equations. The two strains are also assumed to use other resources in the environment and hence saturate at a total population size, which is normalized to 1. Additionally, we recapitulated our daily dilutions by introducing a fixed death rate, $\delta = 0.5$ (although our experiments are done in batch culture, for simplicity we model our mutualism in continuous culture). We incorporated only two aspects of the asymmetry between our two strains. First, based on competition experiments in very high amino acid concentrations (200 & 1600 μM), we calculated that Leu^- has a fitness disadvantage of ~7.5% in optimal conditions (Figure 2.2) so we set the normalized growth rates to be $r_x = 1$ and $r_y = 0.925$. Second, we assume that the Trp- strain contributes more to the mutualism than the Leu^- strain ($\beta = 2$), since the Leu^- strain dominated at intermediate amino acid concentrations (Fig 2.1D).

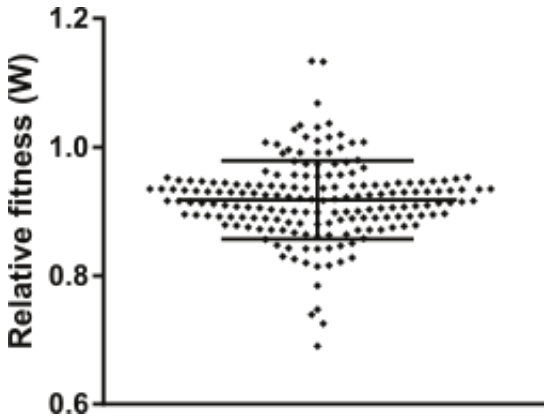

Figure 2.2: Relative fitness of Leu^- is lower than fitness of Trp^-. To analyze fitness difference, we grew the strains in co-culture at saturating amino acid concentrations (200 μM tryptophan and 1600 μM leucine). With such high concentrations, additional amino acids provided through cross-feeding will give negligible benefits, thus enabling us to compare the intrinsic growth rate of the two strains. Co-cultures were started at 36 different combinations of initial density and abundance and grown for two cycles of daily dilution to reach carrying capacity. They were then grown for five additional days, and relative fitness was determined each day in every condition (See section 2.7, appendix). Error bar indicates mean ± s.d.

This simple phenomenological model was able to explain the qualitative regimes of interactions that we observed previously (Fig 2.1D) and suggested that simply by varying the amino acid concentrations we may be able to observe an even larger number of qualitative outcomes between our two strains (Fig 2.3). Increasing amino acid concentrations from the region of obligatory mutualism (O, blue), the model predicts that the interaction should become a facultative mutualism (F, green) followed by a parasitism (P, yellow), with the Leu^- benefiting from the interaction and the Trp- being harmed. The model then predicts that the amensalism previously observed in Fig 2.1D corresponds to the boundary of the parasitism region and a competition region (C, orange), in which the strains coexist but at an equilibrium density below what they would reach in monoculture. This outcome is achieved despite the fact that the force leading to coexistence of the strains is still the sharing of amino acids. Since these strains have complete niche overlap, coexistence is not possible without a stabilizing influence, which is provided by amino acid transfer[48]. At even higher amino acid concentrations the model predicts that the strain with a higher maximal growth rate (Trp^-) should outcompete the slower dividing strain, since in this regime amino acids are no longer limiting (Competitive Exclusion (CE), red). The model also predicts that due to the asymmetry in the strains there will be a small region where the interaction is a facultative mutualism for one strain, yet an obligatory mutualism for the other strain (OF, cyan). Finally, the model predicts that in the absence of supplemented amino acids the mutualism will fail and both strains will go extinct (X, dark blue). This model, although exceedingly simple, therefore predicts the existence of a surprisingly wide range of different qualitative outcomes within a mutualist pair.

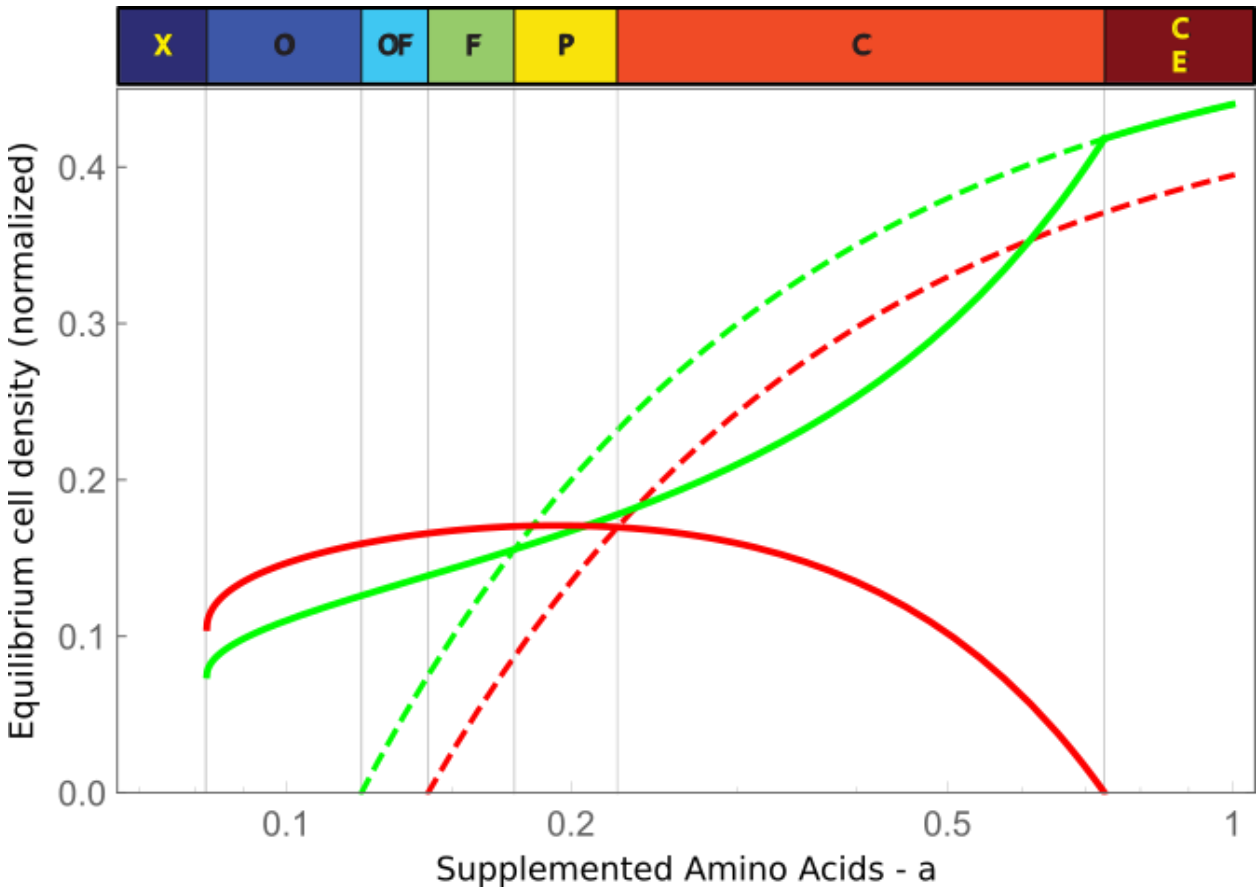

Figure 2.3: A simple phenomenological model predicts that a cross-feeding mutualism can shift between many qualitative outcomes. Plot shows equilibrium density of co-cultures (solid lines) or monocultures (dashed lines) as a function of amino acids. The colorbar above the plot shows the qualitative regimes of interaction. Regimes are extinction (X, dark blue), obligatory mutualism (O, blue), obligatory/facultative mutualism (OF, cyan), facultative mutualism (F, green), parasitism (P, yellow), competition (C, orange) and competitive exclusion (CE, red).

2.4 Testing the Predictions of the Model

To test these model predictions of many different interaction regimes, we experimentally measured the equilibrium abundances at a wide range of amino acid concentrations (Figure 2.4). As predicted by the model, we found that varying the amino acid concentration caused the mutualist pair to switch between seven different qualitative regimes, with the ordering of these regimes as predicted by the model. From low to high amino acid concentrations we observed collapse of the mutualism, obligatory mutualism, obligatory/facultative mutualism (different for

the two strains), facultative mutualism, parasitism, competition, and competitive exclusion (Figure 2.5). A simple model therefore provides remarkably effective guidance in the outcomes that we observe in our experimental microbial cross-feeding system.

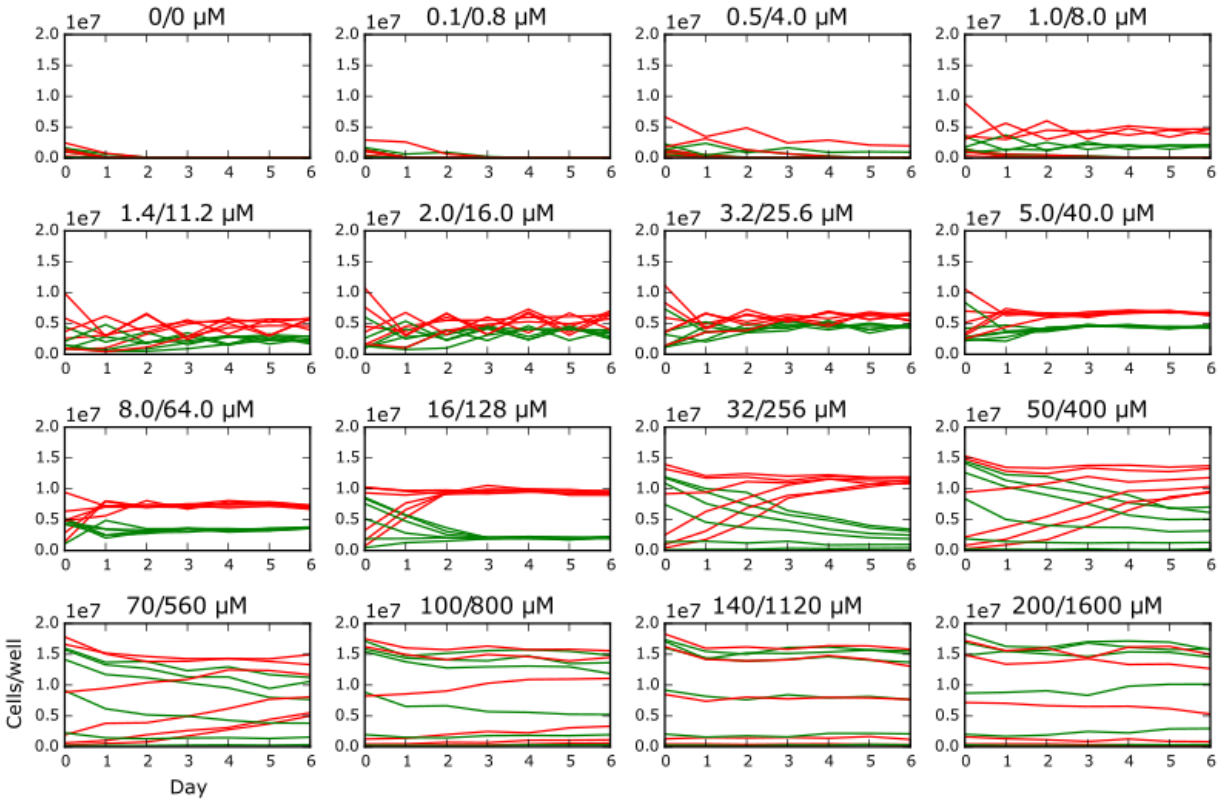

Figure 2.4: Abundances of co-cultures at varying amino acid concentrations. Plots show individuals traces of experiments used for Figure 2.5. Co-cultures were grown at 16 different amino acid concentrations, ranging from 0 μM tryptophan and 0 μM leucine to 200 μM tryptophan and 1600 μM leucine. Co-cultures were started at 6 different relative abundances, and grown for seven cycles of daily dilution. Density of Trp- (green lines) and Leu- (red lines) were measured at the end of each day by spectrophotometry and flow cytometry.

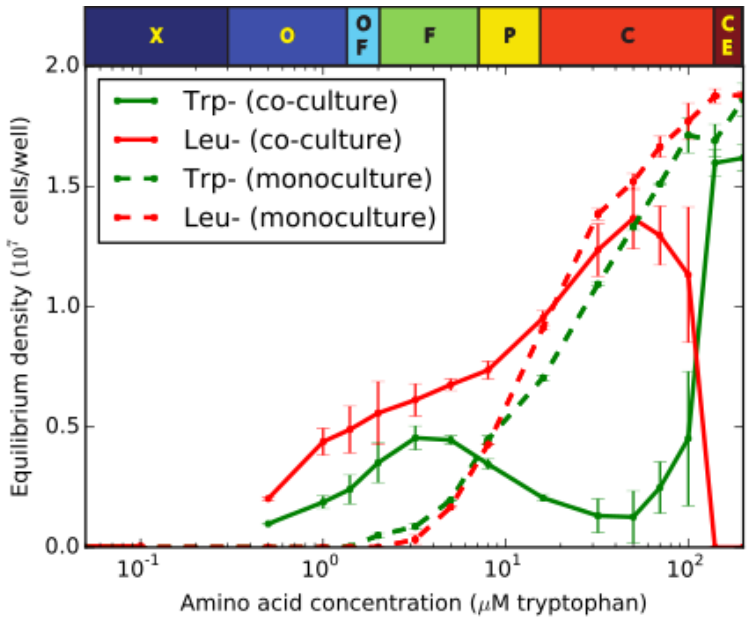

Figure 2.5: Our experimental cross-feeding mutualism shifts between the predicted eight different qualitative outcomes. Co-cultures were grown at amino acid concentrations ranging from 0 to 200 µM Tryptophan and 0 to 1600 µM Leucine. Cultures were started at 6 different fractions and run for 7 days with a 10x dilution each day. In cultures that reached equilibrium (up until 16 & 128 µM), data shows mean density (+- s.e.m), while at higher concentrations mean equilibrium density is estimated by calculating the relative fitness of the two strains as a function of initial fraction (see Figure 2.6). Color bar above the plot shows the qualitative regimes of interaction as in Figure 2.3.

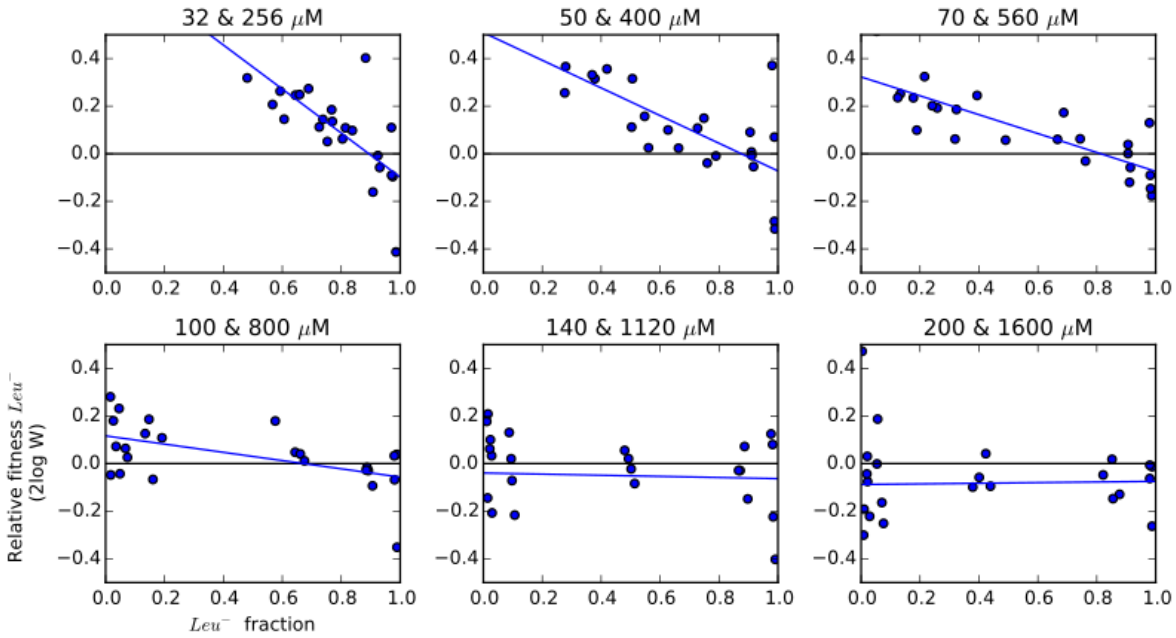

Figure 2.6: estimating equilibrium fractions

Figure 2.6 (continued): Relative fitness as a function of relative abundance. To determine equilibria in co-cultures that had not yet reached saturation, we determined relative fitness as a function of the fraction of Leu- cells. Co-cultures were grown for two days to reach carrying capacity, after which relative fitness was determined as described earlier. Relative fitness was then log transformed and plotted against the fraction of Leu- cells at the start of that day. Bootstrapping was used to determine the equilibrium fraction, at which both strains have the same fitness.

2.5 Characteristic Behavior Before Population Collapse

In both the model (Figure 2.3) and in the experimental system (Figure 2.5), the two strains coexist for intermediate values of supplemented amino acids, but one or both strains go extinct if the amount of supplemented amino acids is either too small or too large. This means, for example, that if the environment were to deteriorate (for example, by decreasing nutrient availability) the system would go through a series of changes in the type of interaction (e.g. parasitism, facultative mutualism) before becoming an obligatory mutualism, and finally going extinct due to the environmental deterioration. Similarly, a rich environment would render the mutualism ineffective, so that the strain with lower fitness would eventually be outcompeted by the other. In principle, knowing the interaction type would indicate whether the system is approaching extinction, although this information requires knowledge of the equilibrium densities for both monocultures and co-cultures, which may not be easily available for many natural systems. However, it is known that a population system close to collapse exhibits a general property referred to as critical-slowing down[17], a fact that we can exploit to characterize the dynamics of the system near two transition points: between the regimes of extinction and obligatory mutualism, and between the regimes of competition and competitive exclusion.

Our model predicts that the approach to equilibrium is very different when the cross-feeding strains interact in an obligatory mutualism as compared to when they interact

competitively (Figure 2.7). Competitively interacting strains rapidly reach carrying capacity, and only later does the ratio of the strains reach equilibrium (Figure 2.7, inset V). In contrast, in the obligatory mutualism regime close to collapse it is the ratio that first reaches equilibrium, and the total population size is the variable that is slow to reach equilibrium (Figure 2.7, inset I). In between these two interaction regimes there is no separation of timescales, and the approach to equilibrium is predicted to be approximately uniform from all directions (Figure 2.7, insets II and III). These changes in dynamics are expected very generally due to critical slowing down, in which the slow relaxation mode is associated with the direction of the eigenvector as the eigenvalue goes to zero (Figure 2.7). The model therefore predicts that just measuring the dynamics of the partner strains allows for an estimate of the kind of interaction, and hence how close the population is to collapse.

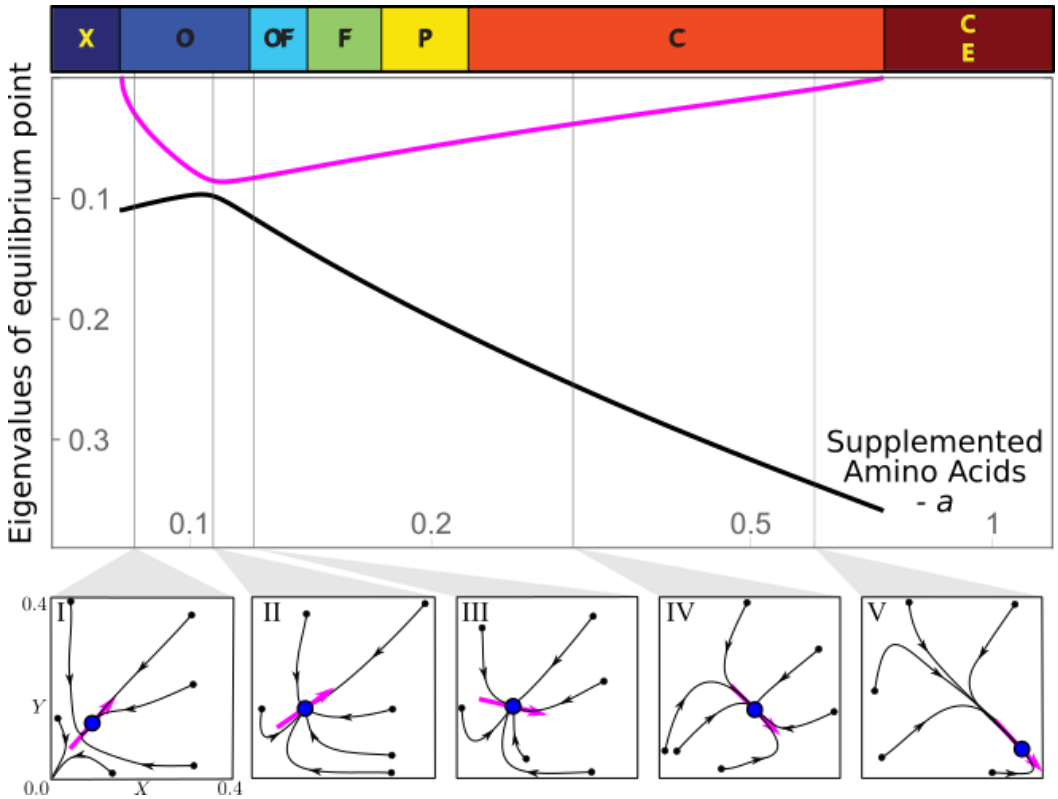

Figure 2.7: eigenvectors and eigenvalues

Figure 2.7 (continued): Eigenvector orientation predicts characteristic behaviors prior to population collapse. Main plot shows eigenvalues as a function of supplemented amino acids. Population collapse occurs when the slower eigenvalue (magenta solid line) reaches zero. Insets I-V show simulated population trajectories (arrowed lines) for different amino acid concentrations, and starting from different population densities (small black dots). The eigenvector (magenta arrow) of the stable equilibrium point (blue dot) corresponds to the slower eigenvalue. Insets show that trajectories align to the eigenvector when the system is close to collapse. This indicates that the ratio of the densities of each strain within the population (i.e. $f = X/Y$) relaxes faster than the total population size (i.e. $N = X + Y$) when the system is close to extinction (inset I), whereas the opposite scenario occurs before the competitive exclusion regime (inset V).

In order to test these model predictions, we measured the dynamics of co-cultures initialized at a wide range of population sizes N and starting fractions f, spanning four and eight orders of magnitude respectively (Figure 2.8). In accordance with the predictions of the model, in high amino acid concentrations (32 μM Trp & 256 μM Leu), the interaction is competitive (Figure 2.8C) and we observed rapid convergence of N, whereas f did not equilibrate even after five days. In contrast, in low amino acid conditions (1 μM Trp & 8 μM Leu, Fig. 2.8A), the interaction is an obligatory mutualism and the cross-feeding interaction resulted in a strong stabilizing effect on the relative abundances[39], with the populations rapidly reaching a 1-to-1 ratio (i.e. $f = 1$). As f equilibrated, the fate of the populations depended on the population size N: those that started at sufficiently high abundance slowly increase their total population size to the equilibrium point value, whereas populations that started too small or imbalanced were fated to extinction ($N = 0$). We were therefore able to experimentally observe the two different separations of timescale predicted by the model in the two different extreme regimes of interaction. Finally, we found that at intermediate amino acid concentrations (8 μM Trp & 64 μM Leu) there was a balance between the two relaxation timescales, thus causing the trajectories to converge to equilibrium from all directions (Fig 2.8B) as predicted by the model (Figs. 2.7-II and 2.7-III). Therefore, the relaxation dynamics of the cross-feeding partners is an early-warning indicator of population collapse.

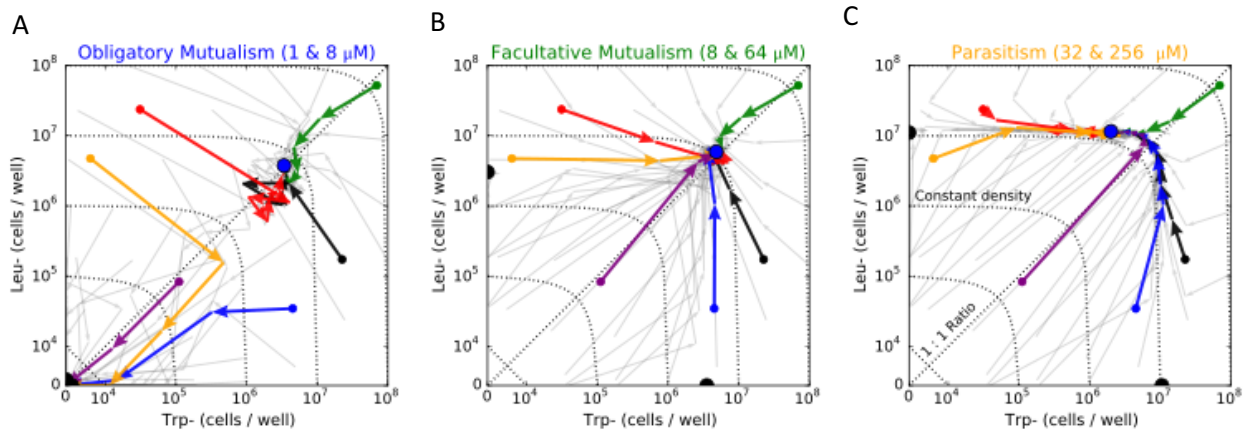

Figure 2.8: Relaxation dynamics is observed before population collapse. In each figure, we started co-cultures at 48 different population sizes ($N = X + Y$) and relative abundances ($f = X/Y$). Six co-cultures per figure are highlighted (colored arrows), with day 0 density represented by a colored dot, and each arrow signifying the change over a single day. Black dots on the axes indicate monoculture equilibria, whereas the blue dot is the co-culture equilibrium. (A): In obligatory mutualistic conditions, close to extinction, populations approach equilibrium from the direction corresponding to constant ratio, f. (B): In medium amino acid concentrations, there is no privileged direction for approaching equilibrium. (C): At high concentrations, when the two strains compete against each other, the population approaches equilibrium from the constant N manifold.

2.6 Discussion

We have established an experimental system that captures a multitude of interactions by simply varying the amount of nutrients available to two partners in a cross-feeding mutualism. Although it is tempting to conclude that this cross-feeding interaction should be an obligatory mutualism, we demonstrate experimentally that the interaction varies greatly with the environment. Depending upon the environment we found that our cross-feeding strains could interact as an obligatory or facultative mutualism, parasitism, amensalism, or competition. A simple phenomenological model explained this range of outcomes, which we view as a significant success given that many models of mutualisms have difficulty shifting between such qualitatively different outcomes; indeed, the Lotka-Volterra model of interspecies interactions fails to even describe an obligatory mutualism without leading to ever-expanding populations[49].

Moreover, the model predicts different relaxation time scales on the brink of collapse that have been confirmed in our experimental system.

Our experiments and modeling suggest that the interaction becomes increasingly cooperative as the environmental quality deteriorates via decreasing nutrient availability. This result is consistent with work done on a range of other mutualisms and interspecies interactions. For example, a global analysis of plant interactions concluded that interactions were typically competitive in benign environments at low elevation, whereas the interactions become increasing facilitative in the more challenging environments present at high elevation[50]. Similarly, the mycorrhizal mutualism has been demonstrated to become parasitic in the absence of abiotic stresses[51]. More generally, the mutualism–parasitism continuum hypothesis[52] posits that a number of environments may cause a mutualism to degrade into a parasitic interaction. Our work in some way echoes these previous findings, but our results also indicate that mutualisms can in some cases shift between an even wider range of possible outcomes.

Our experiments show an interesting asymmetry between the strains, where Leu^- cells dominate at low amino acid concentrations but are competitively excluded at higher amino acid concentrations. Our modeling suggests that this difference is because the Trp^- cells are more "cooperative" (giving the Leu- cells an advantage when amino acids are scarce) but also have an inherent growth advantage when amino acids are not limiting. These differences could be partly due to a difference in adaptation. Adaptation to low amino acid concentrations resulted in better growth at low density but lower maximal growth (Figure 2.9)[43]. It is possible that Leu^- cells were more adequately adapted than Trp^- cells, resulting in better growth in harsh environments but reduced fitness in optimal conditions.

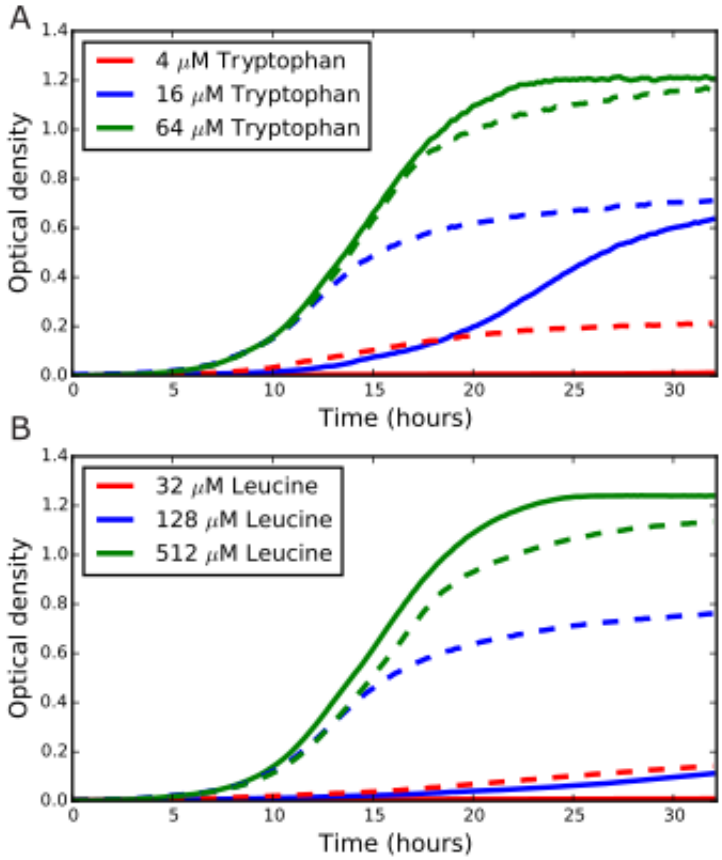

Figure 2.9: Growth curves of *S. cerevisiae* strains before and after adaptation to low amino acids. Trp^- (A) and Leu^- (B) cells in exponential phase were seeded in 96-well flat bottom plates and incubated at 30°C for 32h. Density was measured automatically every 10 minutes through spectrophotometry. Cells were either adapted (dashed lines) or not adapted (solid lines) to low amino acid concentrations by 7 days of growth-dilutions cycles with low amino acid supplementation. At the lowest amino acid concentrations (red lines), adapted strains grew much better than unadapted strains. At medium amino acid concentrations (blue lines), adapted strains still grow better than unadapted strains, although the unadapted Trp^- strain might still reach the same carrying capacity. Interestingly, at high amino acid concentrations (green lines), unadapted strains grow better than adapted strain, suggesting a fitness trade-off between growth in low and high amino acid concentrations.

In this paper we have focused on the interactions between two auxotrophic strains, each of which produces the amino acid needed by its partner. However, in principle this cross-feeding mutualism can be invaded by other strains, the most relevant of which would be the double-producer (producing both tryptophan and leucine) and the non-producer (auxotroph for leucine and tryptophan). At least within the realm of our model, we predict that at intermediate amino

acid concentrations the mutualism is non-invadeable by either of these alternative strains (Figure 2.10 and Appendix 2.6). However, at higher amino acid concentrations the non-producer is predicted to invade and coexist with the single producers (and similarly at lower amino acid concentrations the double producer is predicted to invade). It would be interesting to explore further the degree to which cross-feeding can stabilize the coexistence of multiple strains, particularly given the wide range of nutrients that can be shared in a microbial community.

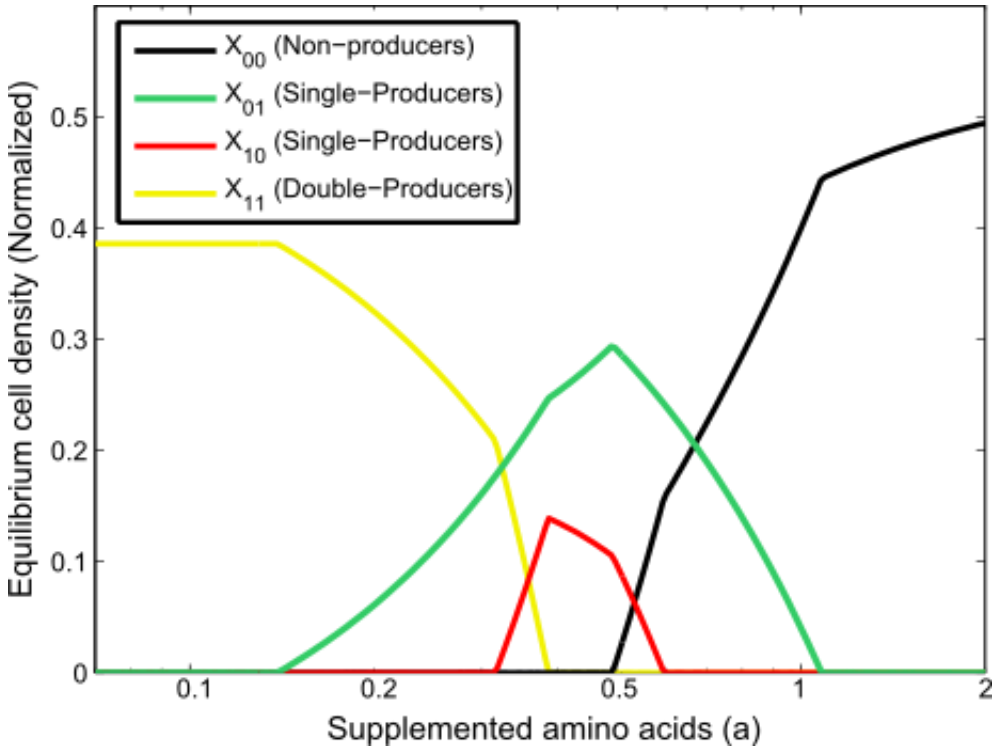

Figure 2.10: A cross-feeding mutualism can protect against invasion by other strains. Plot shows equilibrium density of simulations with four strains as a function of supplemented amino acids. Double producers (yellow line) are modelled to have a lower growth rate than single producers (red and green lines, equivalent to strain X and Y in eq. 1 and 2), while non-producers (black line) have a higher growth rate than single producers (Appendix 2.6). However, double producers produce both amino acids and thus do not benefit from extra amino acids. Non-producers produce no amino acids, and are therefore completely dependent on amino acids provided in the medium or by other strains.

One important feature of our mutualism is that the two strains are almost genetically identical. This means they have near perfect niche overlap, which results in very strong

competition between the two strains. In many other mutualisms the partners will have less niche overlap and will therefore experience less competition. Incorporating this in our model predicts that the degree of niche overlap will have a strong influence on the outcome of the interaction and the degree to which different environmental conditions will switch the nature of the interaction (Figure 2.11). As perhaps expected, less niche overlap results in a larger range of parameters in which the species are mutualistic. Future studies in the field and in the laboratory will be needed to elucidate whether the wide range of interactions observed here are relevant for other mutualisms.

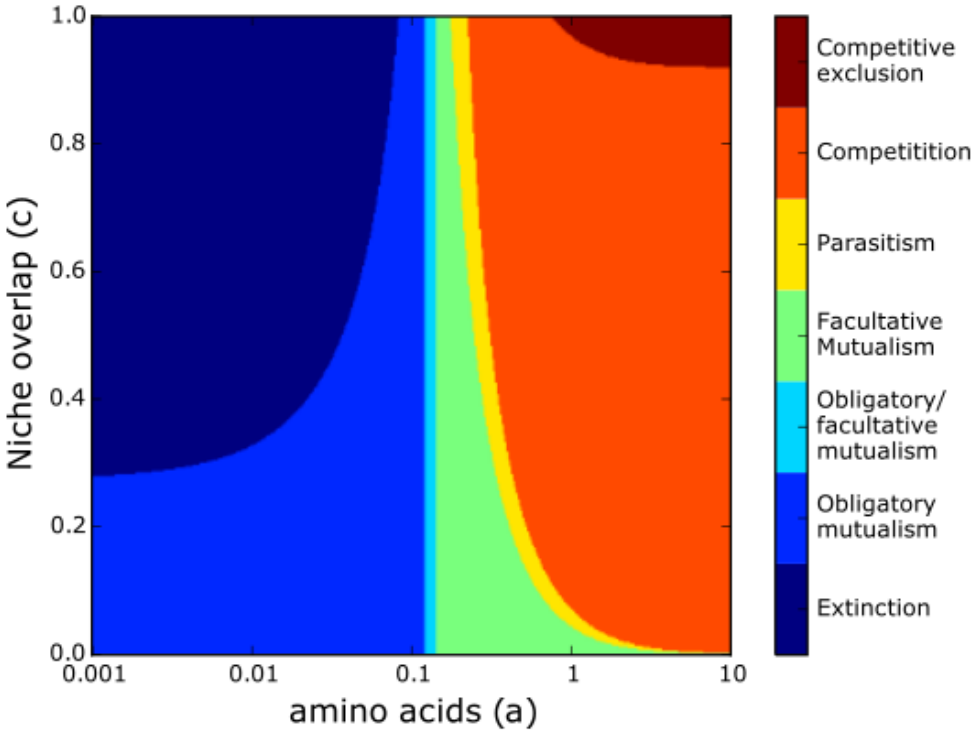

Figure 2.11: Smaller niche overlap results in larger regions of mutualistic interaction. Simulations were run to determine qualitative interaction as a function of supplemented amino acids (a) and niche overlap (c). Niche overlap was modelled as the degree to which each strain affects the carrying capacity of the other strain (S1 information), with c=1 being complete overlap and c=0 being no niche overlap. Although the order of qualitative regimes remains unchanged, not all regimes are present with lower niche overlap, and smaller niche overlap generally results in a larger region of mutualistic interactions

2.6 Appendix: Strains and Methods

Strains and growth media

Both *S. cerevisiae* strains are from a W303 background and are genetically modified to cross-feed as previously described[40]. The strains were adapted to growing with low amino acid supplementation through seven cycles of daily dilution and growth in 2 μM tryptophan and 32 μM leucine. Monoclonal lines derived through plating on 1.5% agarose plates were used for all experiments except for comparison with unadapted strains. Strains were grown in batch culture in synthetic medium, consisting of Yeast Nitrogen Base (YNB, Sunrise Sciences), Complete Supplement Mixture lacking leucine and tryptophan (CSM-leu-trp, Sunrise Sciences) and 2% glucose. Synthetic medium was supplemented with varying amounts of amino acids as indicated in experiments. All daily dilution experiments were performed in BD Falcon 96-well flat bottom plates. Cells were grown in 200 μl batch culture at 30°C, and mixed by a shaker rotating at 900 r.p.m.. Plates were sealed with Bemis Laboratory Parafilm to prevent evaporation.

Co-culture experiments

At the start of each co-culture experiments, single colonies were grown for 24h until saturation in 3 ml synthetic medium containing 100 μM tryptophan and 1000 μM Leucine. They were then diluted by a factor 10 and grown for 4h to prevent cells from being in stationary phase at the start of the experiment. Cells were spun down and washed three times to remove any excess amino acids. Leu^- and Trp^- cells were then mixed in appropriate ratio's and seeded in BD Falcon 96-well flat bottom plates in 200 μl medium. A daily dilution cycle consisted of 23.5h of growth, after which density was measured by spectrophotometry (Thermo Scientific VarioSkan Flash Multimode Reader) and relative abundance was measured by flow cytometry (Miltenyi

MACSQuant VYB, minimum of 10,000 cells analyzed). Cultures were then diluted by a factor 10 into new 96-wells plates containing fresh medium.

Model analysis

Figures 2.3 and 2.7 have been obtained by computing analytical formulae for the equilibrium point, eigenvalues and eigenvectors of Equations [1] and [2]. Simulated trajectories in insets in Figure 2.7 have been obtained by Gillespie simulations[28] of the corresponding stochastic model of Equations [1] and [2].

Calculating relative fitness

Relative fitness is calculated by comparing growth rates of both strains, and is given by the equation:

$$W = r_1 / r_2, \qquad [3]$$

where r_1 is the growth rate of the less fit strain (Leu^-) and r_2 is the growth rate of the fittest strain (Trp^-). The relative fitness of the fittest strain equals 1, the fitness of less fit strains is smaller than 1. Growth rate was determined by comparing densities at the start and end of each dilution cycle. Starting densities were calculated by dividing final density of the previous day by 10, since we diluted by a factor 10. Since yeast growth exponential, growth over the entire 24 hours can be modelled by:

$$N_1(t) = N_1(0)\, e^{r_1 t} \qquad [4]$$

In this model, $N_1(t)$ and $N_1(0)$ represent the densities at timepoint t or timepoint 0, t represents the full 24 hours of growth and r_1 represents the average growth rate over the course of the day. The cultures might be saturating, so the average growth rate will decrease if we let all the

cultures grow for a longer period of time. However, the strains are grown in co-culture so saturation should be equal between strain, and therefore not affect fitness of either strain. r_1 can be isolated from equation 4 and is given by equation 5:

$$r_1 = \ln(\frac{N_1(t)}{N_1(0)}) \qquad [5]$$

Since $N_1(0)$ and $N_1(t)$ are the initial and final density of each day, which we acquire from our data, we can now calculate the average growth rate. Note that the absolute values of r_1 and r_2 are not important, because we only wish to compute the relative fitness, and that the values should therefore not be compared to the growth rates in equation 1 and 2. The relative fitness W is then calculated by dividing r_1 by r_2 (equation 3).

Estimating equilibrium densities when cultures have not reached saturation.

Since co-cultures did not reach equilibrium density within 7 days at high amino acid concentrations (above 32 μM tryptophan & 256 μM leucine, Figure 2.4), we estimated equilibrium densities by determining relative fitness as a function of relative abundances. We determined fitness of Leu^- as described above in equation 3, and plotted the log(2) transformed fitness against the fraction of Leu^- cells. At a low fraction of Leu^- cells, Leu^- cells will have a fitness advantage over Trp^- cells because of the nutrients provide by Trp^-, and vice versa. However, when the strains are at equilibrium fraction they will have equal fitness (since abundance does not change anymore). We used bootstrapping to calculate at which fraction the cells had equal fitness. We ran a simulation in which we randomly resampled our data (with replacement) 100,000 times. In each resampling, we fitted a first degree polynomial and calculated the Leu^- fraction at which fitness was equal. Equilibrium fractions below zero were

rounded up to zero, and fractions above one were rounded down to one. We then calculated the mean equilibrium fraction (+- s.e.m.) of these simulations.

To estimate the equilibrium density of both strains, we combined data of equilibrium fraction and equilibrium total density. We assumed that at these high amino acid concentrations, co-cultures will reach equilibrium total density within a few days, and therefore calculated the variation in total density similar to saturated co-cultures (mean +- s.e.m. of the means of six conditions over the last three days). Equilibrium density of individual strains was calculated by multiplying equilibrium density with equilibrium fraction. Standard error of the mean of densities of individual strains was calculated by the formula:

$$SE_f \approx \sqrt{B^2 SE_a^2 + A^2 SE_b^2} \qquad [6]$$

In which SE_f is the standard error of the mean of the density of one strain, A is the total density, B is the equilibrium fraction of that strain, and SE_a and SE_b are the s.e.m. of total density and equilibrium fraction. The standard deviations calculated with equations 6 are depicted in Figure 2.5.

Modeling of interactions between four species.

To analyze the behavior of our system in the presence of other species, we extended our model to a four-species system. This system includes the two initial cross-feeding strains, which are given in this model by X_{01} and X_{10}. The strain X_{01} (which is Trp^- or strain X) does not produce the first nutrient (tryptophan), but does produce the second nutrient (leucine), while strain X_{10} (Leu^- or Y) produces the first but not the second nutrient. The two new strains are X_{11}, which produces both

nutrients, and X_{00}, which produces no nutrients. Equilbrium densities are calculated with the following equations:

$$\frac{dX_{00}}{dt} = X_{00}\left(\frac{X_{10}+X_{11}+a}{X_{10}+X_{11}+a+\kappa}\right)\frac{\beta X_{01}+X_{11}+a}{\beta X_{01}+X_{11}+a+\kappa}(1-X_{00}-X_{01}-X_{10}-X_{11})-\delta X_{00} \quad [7]$$

$$\frac{dX_{01}}{dt} = (1-c_1)X_{01}\left(\frac{X_{10}+X_{11}+a}{X_{10}+X_{11}+a+\kappa}\right)(1-X_{00}-X_{01}-X_{10}-X_{11})-\delta X_{01} \quad [8]$$

$$\frac{dX_{10}}{dt} = (1-c_2)X_{10}\left(\frac{\beta X_{01}+X_{11}+a}{\beta X_{01}+X_{11}+a+\kappa}\right)(1-X_{00}-X_{01}-X_{10}-X_{11})-\delta X_{10} \quad [9]$$

$$\frac{dX_{00}}{dt} = (1-c_1-c_2)X_{00}(1-X_{00}-X_{01}-X_{10}-X_{11})-\delta X_{11} \quad [10]$$

The growth rate of each strain increases with the abundance of the amino acids they cannot produce. Amino acids can be acquired from supplementation (a) or from mutualist partners (X_{11}, X_{10} or X_{01}), and again saturate via a Michaelis-Menten form with the same scaling constant (kappa = 0.12). We also maintained the unequal contribution to the mutualism ($\beta = 2$). Since all species have the same nutrient requirements apart from leucine and tryptophan, they saturate at a carrying capacity that is normalized to 1. The cost of producing nutrients is modelled by a cost that reduces the growth rate. The growth rate of the non-producer, which does not produce amino acids and thus has no costs, is normalized to 1. We modelled a different cost of producing each nutrient ($c_1 = 0.10$ and $c_2 = 0.1675$), so that the growth rate of strain X_{10} remains 0.925 times that of strain X_{01} (0.8325 / 0.90 = 0.925). Since the double-producer makes both nutrients, its growth rate is reduced by c_1 and c_2 (1 – 0.10 – 0.1675 = 0.7325). To compensate for the reduced growth rates compared to our original model, we normalized the death rate by a factor ($1 - c_1 = 0.9$), resulting in a death rate of $\delta = 0.45$.

Modelling niche overlap

In our standard model (eq. 1 and 2), we assumed complete niche overlap, since both yeast strains are identical except for a few genetic modifications. This means they require the exact same nutrients (apart from leucine and tryptophan), and their growth is thus limited equally by saturation of either strain, which we modelled as (1 – X – C). However, if the two strains do not require the exact same nutrients, e.g. when one strain grows on glucose and the other strain grows on sucrose, there will not be complete niche overlap. In this case, one strain could still grow even when the other strain has reached carrying capacity. We modelled this by introducing niche overlap 'c' into the saturation term. This way, strain X saturates by (1 – X – cY), and strain Y saturates through (1 – cX – Y):

$$\frac{dX}{dt} = r_x X \left(\frac{Y+a}{Y+a+\kappa}\right)(1 - X - cY) - \delta X \qquad [11]$$

$$\frac{dX}{dt} = r_x X \left(\frac{Y+a}{Y+a+\kappa}\right)(1 - X - cY) - \delta X \qquad [12]$$

Qualitative interactions were determined by running simulations with different values of a and c. Simulations were started with abundances of both strains above carrying capacity.

Chapter 3

The Allee Effect and Evolutionary Rescue

Natural populations frequently face harsh environments in which their death rate exceeds their birth rate and population size tends toward zero. In such scenarios, populations can either go extinct, migrate to a region of better habitat, or undergo evolutionary rescue, in which evolutionary adaptation allows the population to survive. Natural populations often exhibit an "Allee effect," in which populations grow slowly at low density due to struggles with such behaviors as finding a mate or collective hunting. We hypothesized that the presence of an Allee effect could impede evolutionary rescue and confirmed this hypothesis in a model laboratory yeast population. We compared extinction rates in glucose (no Allee effect) and sucrose (strong Allee effect) in a high salt environment and found that populations in glucose underwent evolutionary rescue in an environment where sucrose populations went extinct, in spite of sucrose populations starting from a larger population size and having a larger carrying capacity. We show that after several days of growth in a harsh environment, cells in sucrose which will eventually go extinct can be reinoculated at a high density and survive ecologically in an environment which their unevolved ancestors could not. Our results represent a striking example of eco-evolutionary feedback and highlight how the Allee effect can influence conservation efforts.

3.1 Motivation and background

Species in nature are currently going extinct at an alarming rate due to global climate change[53,54]. When a population encounters an environment to which it is poorly adapted and death rate exceeds birth rate, three things can happen: extinction, migration to a region of better habitat, or

adaption (either phenotypic adaptation through changing behavior or genotypic adaptation through changing genetic structure). The process by which a population alters its genetic structure to avert extinction is termed "evolutionary rescue." Evolutionary rescue events are characterized by a U-shaped trajectory on a plot of population versus time: the population first declines, then stabilizes, and finally increases.

Much theoretical work has focused on different factors influencing if and how populations undergo evolutionary rescue[55–58], but experimental work has only recently begun to test these ideas. Bell and Gonzalez have pioneered the use of laboratory yeast populations to study evolutionary rescue in high salt environments: they first investigated how initial population size influences the probability of evolutionary rescue[59], and they later extended this work to spatially connected metapopulations[60] and multispecies soil communities[61]. Kerr and colleagues have studied evolutionary rescue under different rates of environmental deterioration[62], while Zhang et al have investigated evolutionary rescue under temporally fluctuating selection pressures[63]. Together, these studies using viruses, bacteria, and yeast have shed much light on evolutionary rescue. However, an underappreciated factor which could affect the probability of evolutionary rescue is the presence of an Allee effect.

The Allee effect refers to a positive correlation between population size and per-capita population growth rate[64]. Allee effects can arise in small populations due to the need for collective defense, group hunting, or finding a reproductive partner[65]. Allee effects are believed to be common in natural populations ranging from plants[66] to mongooses[67] to zooplankton[68]. We hypothesized that the presence of an Allee effect in a population could hinder evolutionary rescue. This is because, during population decline in a harsh environment, the population size could fall below the "Allee threshold" into a regime of particularly slow population growth. We

sought to compare two populations with different strength Allee effects each undergoing decline in a harsh environment. With laboratory yeast as our experimental organism, we used salt to modulate the quality of the environment and used sugar metabolism (glucose or sucrose) to tune the strength of cooperative interactions in the population[69]. We found that the populations growing on sucrose that experienced the Allee effect were much less able to survive the harsh environment via evolutionary rescue.

3.2 Computational Simulations

To assess the plausibility of our hypothesis, we first conducted stochastic tau-leaping computational simulations of yeast populations in glucose and sucrose in a harsh environment. Populations were initially growing in a benign environment before suddenly switching to a harsh environment. In our simulations, populations were initially composed of cells that are poorly adapted to the high salt environment, and beneficial mutants with a higher growth rate arose stochastically during the simulation (see Section 3.6 for details of the simulations). We modeled the growth in glucose as logistic, and growth in sucrose as biphasic. Mathematically in sucrose, the growth can be described as:

$$\frac{dN}{dt} = \gamma_{high} N \left(1 - \frac{N}{K}\right) - \delta N \quad for\ N > N_{crit}$$

$$\frac{dN}{dt} = \gamma_{low} N - \delta N \quad for\ N < N_{crit}$$

Here N is the total population size, K is the carrying capacity, δ is the death rate, and we approximate the growth as biphasic characterized by two different γ above and below a critical threshold.

As we increased the death rate in our simulations, the populations passed through three distinct regimes (Figure 3.1):

I. Ecological survival, in which the cells could outrun the death rate without any evolution

II. Evolutionary rescue, in which the cells would initially tend toward extinction but would avoid extinction due to adaptive evolution

III. Extinction, in which adaptive evolution could not occur rapidly enough to prevent the population size from going to zero

Figure 3.1: simulations show region of evolutionary rescue is much wider in glucose than in sucrose. Populations grew for 40 hours before shifting suddenly to a harsh environment with death rate d (x-axis). Death rate was increased in steps of .01 and 10 replicates were done at each death rate. Fraction of replicates surviving is plotted on y-axis. Growth was logistic in sucrose and biphasic in sucrose. Each trajectory was classified as ecological survival (birth rate of ancestral population > death rate), evolutionary rescue (birth rate of ancestral population < death rate, yet mutants sweep fast enough to enable survival) or extinction.

There are three key aspects of Figure 3.1 that we would like to highlight. First, we observed ecological survival in sucrose at a death rate (d=1.02) where evolutionary rescue was needed for survival in glucose. Second, the range of death rates where we observed evolutionary rescue (yellow bar, top of figure) was much wider in glucose than it was in sucrose. Third, we observed evolutionary rescue in glucose at a death rate (d=1.07) where only extinction was seen

in sucrose. Taken together, these results indicate that evolutionary rescue is possible in a much wider range of harsh environments in glucose than in sucrose. This is driven by the fundamentally different nature of the growth dynamics at low population density, rather than the cells "being happier" or "growing faster" with glucose as a carbon source.

To highlight the difference in outcomes in the difference sugar environments, we compared the population trajectories when d=1.07 (Figure 3.2). In glucose, the populations decreased in size for several generations (Figure 3.2A). As beneficial mutants arose and began sweeping through the population, the rate of decline slowed before eventually ceasing. The population then recovered and stabilized at a lower carrying capacity. In contrast, the populations in sucrose declined similarly before eventually going extinct (Figure 3.2B). In both sugar environments, the mutant eventually reached fixation (Figure 3.2C and 3.2D). Extinction in sucrose occurred despite the fact that the population in sucrose started from a higher total population size than the population in glucose (all other things equal this larger population size should facilitate evolutionary rescue as it provides a larger number of cells that could possibly acquire the mutation will allow for survival in the harsh environment). The two sugar environments display qualitatively different outcomes due to the presence of an Allee effect in sucrose, which dramatically hinders growth in the regime of low population size. These simulations indicated that an Allee effect might indeed hinder evolutionary rescue, which led us to pursue experiments with laboratory yeast to further test our hypothesis.

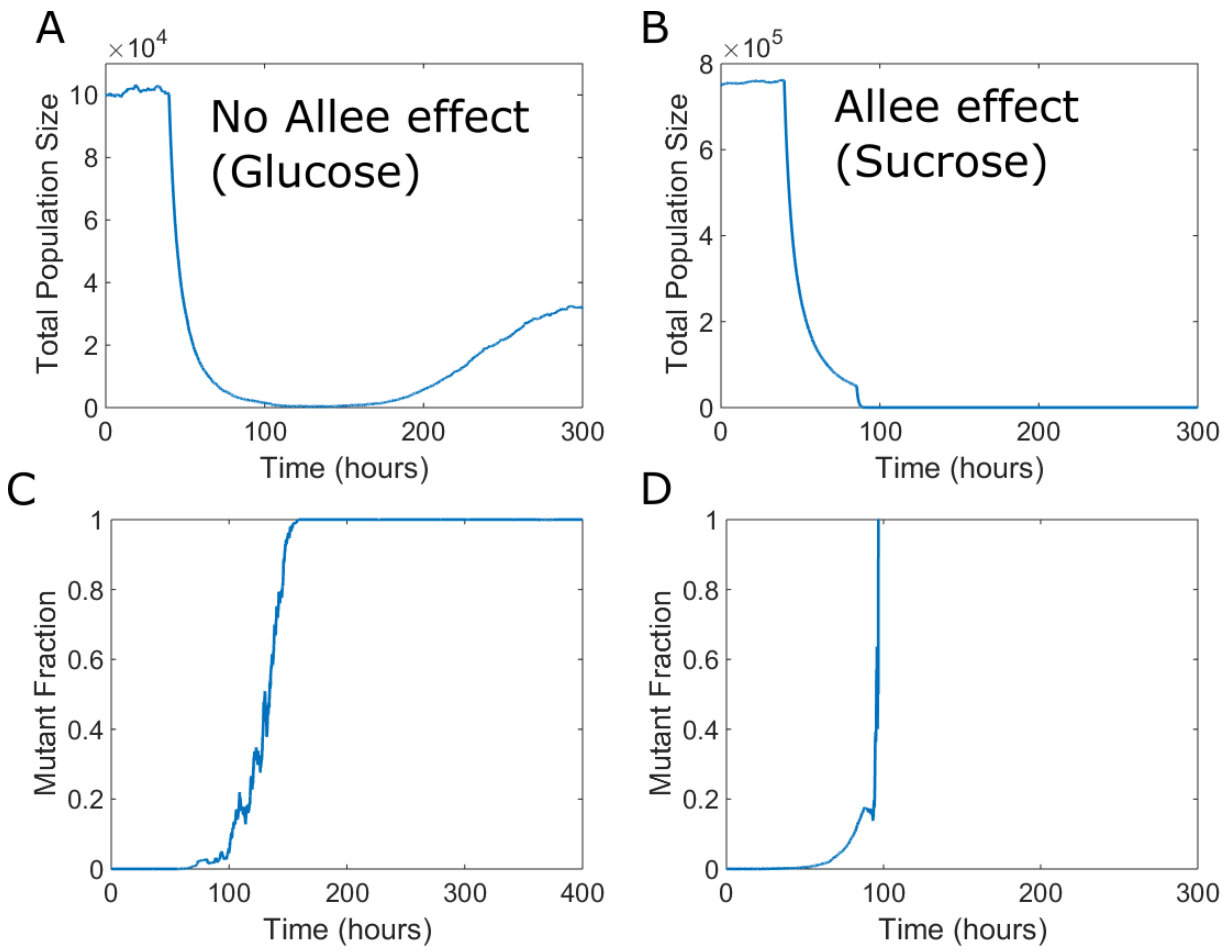

Figure 3.2: Stochastic simulations show different trajectories in glucose and sucrose. Cells grew for 40 hours in a benign environment before suddenly shifting to a harsh environment. Total population size is plotted as a function of time in **A)** glucose and **B)** sucrose. There are two subpopulations, an ancestral population and a mutant population with a 10% fitness advantage. The population is initially composed at t=0 purely of ancestral cells. Cells mutate with a rate $\mu=10^{-6}$. Growth in glucose is logistic. Growth in sucrose is biphasic; above the Allee threshold, growth is logistic, while below the threshold the growth rate grows linearly with the population size. Mutant fraction as a function of time is plotted in **C)** glucose and **D)** sucrose.

3.3 Experiments in Glucose and Sucrose

We first sought to observe evolutionary rescue in yeast populations growing in glucose. We grew the cells in liquid batch culture with daily dilution of 10X into fresh media (corresponding to a 90% daily mortality rate). This created a scenario in which, if the cells could not divide faster than every 7.2 hours, they would fail to keep pace with the daily dilution rate

and eventually go extinct. Controlling the concentration of glucose and sodium chloride in the growth media enabled us to control the quality of the environment.

In our pilot experiments, we struggled to observe rescue events. We hypothesized that this was because our populations had insufficient genetic diversity. To ameliorate this issue, we allowed our yeast populations to accumulate mutations by growing them for 150 generations in a low-salt environment. Our goal was to give the population time to generate a broad distribution of mutations. We took 10^6 cells from this population and grew them up in a medium salt environment so that they would activate their osmotic stress response genes[7]. This was done to ensure that the cells were phenotypically adapted to a high salt environment, so that we could focus on genomic evolution rather than changes in gene expression.

We first demonstrated that these yeast populations in glucose would indeed exhibit the three dynamic regimes (ecological survival, evolutionary rescue, and extinction) in response to increased amounts of sodium chloride (Figure 3.3). In a low salt regime (1000 mM), the cells were initially seeded at a range of population sizes above, at, and below the carrying capacity. Regardless of the initial density, the populations quickly tended toward the carrying capacity (Figure 3.3, top left panel). In a medium salt environment (1135 mM), if the cells were seeded at a high density, the population fell sharply for the first three days before stabilizing and recovering (Figure 3.3, top right panel). If the populations were seeded at a lower density, populations in this environment went extinct. We hypothesize that this dichotomy arises because small populations contain an insufficient number of strongly beneficial mutants, consistent with what other researchers have found regarding the importance of starting population size for evolutionary rescue[59]. In a high salt environment (1165 mM), the cells went extinct regardless of the initial population size (Figure 3.3, bottom left panel). Thus, yeast populations in glucose can

alter their genetic structure sufficiently to survive a poor quality environment with a 90% daily mortality rate.

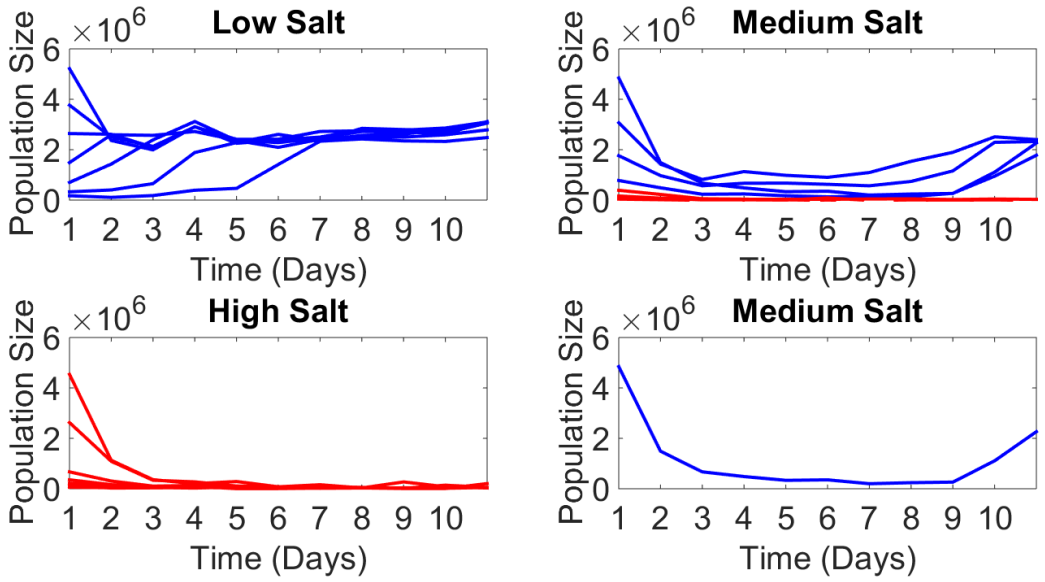

Figure 3.3: Cells in glucose exhibit ecological survival, evolutionary rescue, and extinction. Cells were pre-grown in 700 mM NaCl and 2% sucrose. On day 0, cells were washed and inoculated at a range of densities in .03% glucose supplemented with 1000 mM NaCl ("Low Salt" top left panel), 1135 mM NaCl ("Medium Salt" top right panel), or 1165 mM NaCl ("High Salt" bottom left panel). Cells were subjected to repeated cycles of 23.5 hours of growth at 30°C followed by 10X dilution. Trajectories leading to survival are shaded blue, and trajectories leading to extinction are shaded red. For clarity, one of the "evolutionary rescue trajectories" from the medium salt environment has been plotted alone in the bottom right panel.

We next sought to compare extinction trajectories in glucose and sucrose. We hypothesized that even in a sugar environment where the sucrose cells have a higher carrying capacity and are seeded at a higher population size, we would observe extinction in sucrose in an environment where we had previously seen evolutionary rescue in glucose. We adjusted the quality of the environment by supplementing the sucrose populations with more sucrose than the glucose populations received of glucose (.075% w/v sucrose compared to .03% w/v glucose). We pre-grew the cells in sucrose and salt to activate the expression of invertase and osmotic stress

response genes, and then transferred the two populations to an environment containing 1135 mM NaCl on day 0. The trajectory in sucrose showed three clear phases: rapid decline (days 1 – 4), as the population was initially poorly adapted; a slow decline (days 4 – 8), as beneficial mutants began sweeping through the population; and a rapid decline (days 8 – 11), as the population fell into the low-density regime where the Allee effect predominated (Figure 3.4).

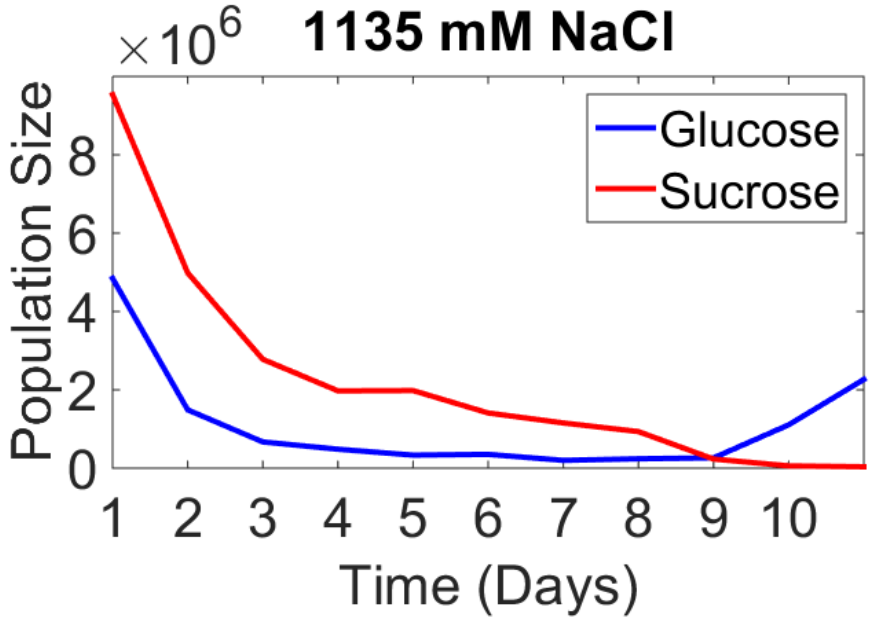

Figure 3.4: in an environment where both glucose and sucrose cells initially trend toward extinction, glucose populations undergo rescue and sucrose cells go extinct. Cells were pre-grown in 700 mM NaCl and 2% sucrose. On day zero, they were washed and transferred to either .03% glucose (blue) or .075% sucrose (red) with 1135 mM NaCl and subjected to repeated 23.5 hour cycles of growth at 30°C and 10X dilution.

Initially, in sucrose, there is only one fixed point in the dynamics: extinction. However, during the experiment, the growth curve shifts due to evolution. If the curve were to shift so that it intersected the death rate curve, a new fixed point would arise, enabling survival (Figure 3.5). If this happened sufficiently quickly, the sucrose cells could undergo rescue and avoid extinction. But if this new fixed point arises after the population has fallen below N_{crit}, the population will go extinct. This leads to a prediction: cells in sucrose that have fallen below the

Allee threshold might have evolved sufficiently so that they could survive in this high-salt environment, if only they could escape the Allee regime and reach a high population size.

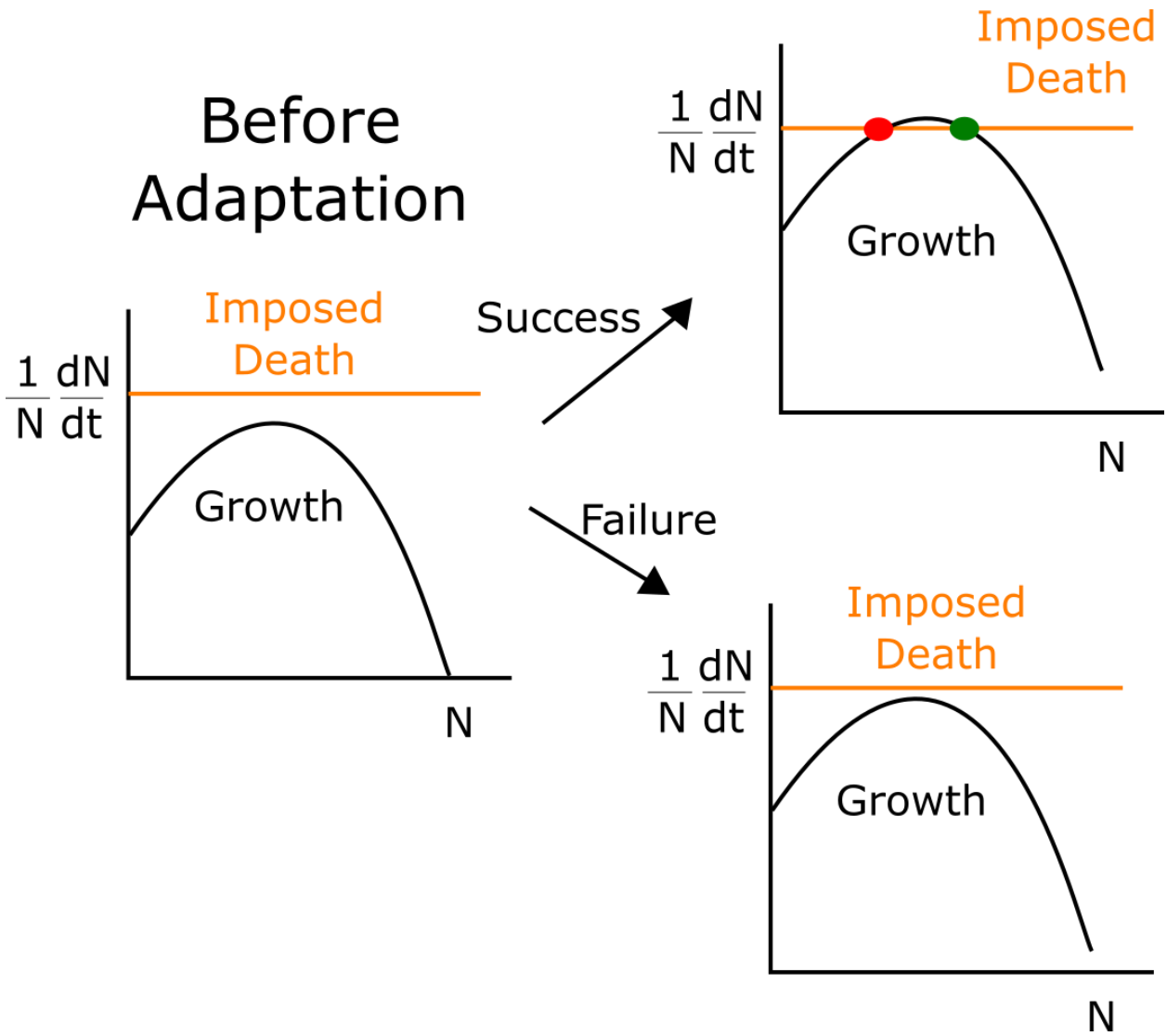

Figure 3.5: The fate of populations depends on the ability of growth curve to rapidly shift upwards. Left: growth and death curves initially do not intersect, so population trends toward extinction. Growth curve shifts upwards over time. When curves intersect (top right), there are two stable fixed points, extinction and survival (green dot) separated by an unstable fixed point (red dot). If N is below the red dot when the two curves intersect, extinction will still occur even though a survival fixed point now exists at a non-zero population size. If adaptation does not occur fast enough, failed rescue (i.e. extinction) results (bottom right plot).

3.4 Reinoculation experiments

To test this prediction, we took sucrose populations from day 9 of the experiment in Figure 3.4 and grew them up to a high density. We then reinoculated them at a range of initial densities in .075% sucrose and 1135 mM NaCl. Prior to the 9 days of evolution this population underwent, the ancestral population could not survive in this environment. In contrast, the evolved cells could survive ecologically in this environment (Figure 3.6). The system is now bistable: populations seeded above a critical threshold will survive, while populations seeded below this threshold will go extinct[16]. Thus, we argue that the ancestral population in sucrose went extinct, not due to the absence of beneficial mutants in the population, but because the mutants failed to sweep through the population before the density fell below the Allee threshold.

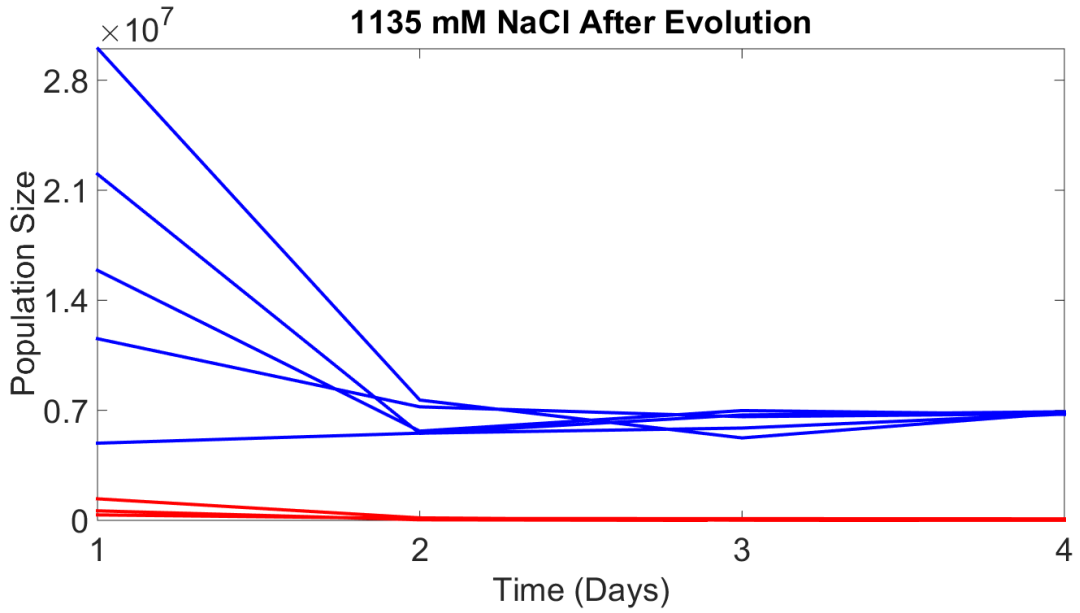

Figure 3.6: Evolved sucrose populations can survive ecologically in an environment where their ancestors went extinct. On day 9 of the experiment in Figure 3.4, cells were transferred to a flask and grown to a high density. After pre-growth in 2% sucrose and 700 mM NaCl, the cells were washed and transferred to media containing .075% sucrose and 1135 mM NaCl on day 0. The populations were then subject to repeated cycles of 23.5 hours of growth followed by a 10X dilution into fresh media.

3.5 Discussion

Here we have used a combination of computational simulations and laboratory experiments to compare population dynamics of yeast growing in glucose (no Allee effect) or sucrose (Allee effect) in a harsh, high-salt environment. We found that populations in sucrose, in spite of having a larger carrying capacity and starting from a larger initial population size, went extinct in a high-salt environment where glucose cells could undergo evolutionary rescue. We further showed that the extinction observed in sucrose populations was not due to a failure of evolution: the populations trending towards extinction survive if inoculated at high density. Extinction in sucrose is therefore driven by the presence of an Allee threshold, rather than a failure of adaptive evolution. We emphasize that these are preliminary results which we will seek to further replicate in future experiments.

We have referred to growth in glucose as "no Allee effect," but in reality the situation is slightly more nuanced than that. Although glucose can be directly imported into the cell and there is no collective breakdown of the sugar, there are in principle other sources of the Allee effect. For example, we have found that there can be an Allee effect even in glucose when the media starts at neutral pH, as the cells collectively acidify the environment[70]. In our experiments we use media that starts at acidic pH, thus minimizing this effect. In addition, there could be a modest Allee effect associated with the population response to the salt stress, as the population secretes and uptakes compatible solutes[71]. Yeast growth in glucose and salt may therefore have a small Allee effect, but not large enough to inhibit evolutionary rescue in the way that it does in the sucrose condition.

Our comparison of rescue trajectories in glucose and sucrose also implicitly assumes that there are comparable numbers of beneficial mutations in glucose and sucrose that would lead to

evolutionary rescue. However, the fitness of a mutation is highly dependent on the environmental context[72]. To further bolster our claim that failure to observe evolutionary rescue in sucrose is driven by an Allee effect (and not simply an absence of beneficial mutants in the population) future experiments will compare the distribution of fitness effects in both glucose and sucrose.

Our results explored one mechanism of environmental deterioration (salt stress) and one mechanism for modulating the Allee effect (cooperative sucrose metabolism). However, we believe that our results should extend beyond this experimental system and be generally true for declining populations which exhibit an Allee effect. The logic underlying our claim is outlined in Figure 3.1; we note that these simulations do not include any information about the environmental stressor or the mechanism of the Allee effect. Future experiments will aim to confirm our hypothesis using other environmental stressors to which a population can be maladapted (e.g. temperature stress, nutrient limitation, antifungal drugs) and other Allee effect mechanisms (e.g. buffering the pH far away from the optimal pH for growth).

As many natural populations tend toward extinction due to the effects of anthropogenic climate change, evolutionary rescue represents a potential strategy for populations to avoid collapse. However, as these populations shrink in size, they could fall into a regime of slow growth due to difficulty with collective defense or finding a mate. Such considerations could force conservation ecologists to reconsider the threshold at which many populations are considered "threatened," "vulnerable," or "endangered."[73] The ubiquity of Allee effects in natural populations underscores the importance of our results for understanding the dynamics of phenomena such as biological invasion and evolutionary rescue.

3.6 Appendix: Methods

Strains

All experiments used a BY4741 strain of yeast which express a constitutive YFP. Cells were pre-grown for 4 weeks in 3 mL of YNB CSM supplemented with 2% glucose and diluted daily by 1000X. Glycerol stocks of this population were stored in 1 mL aliquots at – 80°C, and 100 μL of this glycerol stock was used to start all experiments.

Evolutionary rescue runs

On day minus one, 100 μL of the population described above was inoculated into 3 mL of YNB CSM with 2% sucrose and 700 mM NaCl to induce expression of invertase and osmotic stress response genes. On day zero, cells were washed to remove residual sucrose and salt and then transferred to a 96-well plate with glucose, sucrose, and NaCl as described in the text. Plates were shaken at 30°C and 1000 rpm for 23.5 hours. The optical density was then measured using a Varioskan Flash plate reader, and cells were diluted 10X by transferring 20 μL of cells into 180 μL of fresh media. This was repeated for several days of cycles as described in the text. Extinction was confirmed by letting the cells grow for 3 additional days after the end of experiment and observing that the optical density did not exceed the background threshold of the spectrophotometer.

Reinoculation experiments

On day 9 of the sucrose extinction trajectory in Figure 3.4, 20 μL of cells were transferred to a flask with 2% sucrose and 600 mM NaCl and grown up to high density. Cells were then washed and inoculated at a range of densities in a range of sodium chloride concentrations, most importantly 1135 mM NaCl (the environment in which they evolved and their ancestors went extinct).

Computational Simulations

Tau-leaping simulations were performed in MATLAB. Populations initially grew in a benign environment before being transferred to a harsh environment at t=40 hours. Birth rate was 1, and death rate was .9 in the benign environment. Death rate varied from .9 to 1.19 as described in the text. The population consists of two species, an initially dominant wild-type strain and a mutant population with a 10% fitness advantage in the harsh environment. Time steps were 6 minutes, and the mutation rate $\mu=1*10^{-6}$.

Chapter 4

Conclusion

4.1 Side Projects

During my PhD, I also had the opportunity to play a supporting role in a very interesting project exploring the following question: why do genetically identical cells adopt a range of phenotypes in a homogeneous environment? The most common answer to this question is that the cells are hedging their bets against a sudden and unexpected fluctuation or shift in environmental conditions. Bet hedging has been invoked to explain phenotypic heterogeneity in numerous situations, ranging from persistence to sporulation[74,75].

An alternative, underexplored explanation is that of negative frequency dependent interactions among strategists in a population. To study this question, we used the well-known yeast galactose utilization network as described in chapter one of this thesis. In a mixed sugar environment, a clonal yeast population will adopt a bimodal activation pattern of the galactose utilization genes, i.e. some cells will consume galactose ("GAL ON") and others will not consume galactose ("GAL OFF"). We hypothesized that bimodality could arise from negative frequency dependent interactions between GAL ON and GAL OFF cells, such that the optimal strategy could depend on the strategy of other players in the game. To test this hypothesis, we used genetic mutants in which the network had been altered so that the GAL genes were always on or always off. We competed the pure strategists in a mixed sugar environment (.03% glucose and .05% galactose) starting from a range of initial fractions and measured how the fitness of each strain varied with its initial frequency. The results of this competition are shown in Figure

4.1. We found that the GAL-ON specialist was more fit when it was initially rare in the population, but that this specialist was less fit when it was initially common in the population.

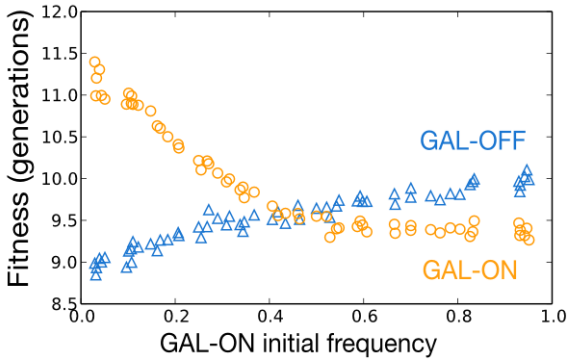

Figure 4.1: GAL-ON and GAL-OFF specialists show negative frequency dependence. Fitness, in number of generations, is shown for the two phenotypes as a function of the population frequency of GAL-ON. The crossing point indicates an evolutionarily stable coexistence of around 40% GAL-ON for this mix of sugars.

My role in the project was two-fold. First, some readers of this work worried that our results were an artifact of our experimental protocol, in which the two strains competed for 20 hours. During this time course, the concentration of sugars in the growth media would change dramatically as the cells consumed them. To assuage these concerns, I conducted similar competition experiments between the pure strategists in a semi-continuous environment in which the sugars were constantly replenished every three hours for several cycles of growth. The results of these experiments are shown in Figure 4.2. We found that in a pure glucose environment, one specialist dominated the other at all initial frequencies. In a mixed sugar environment, there is negative frequency dependence, and the plot of initial frequency versus relative fitness crosses unity, indicating stable coexistence at intermediate frequencies in this environment.

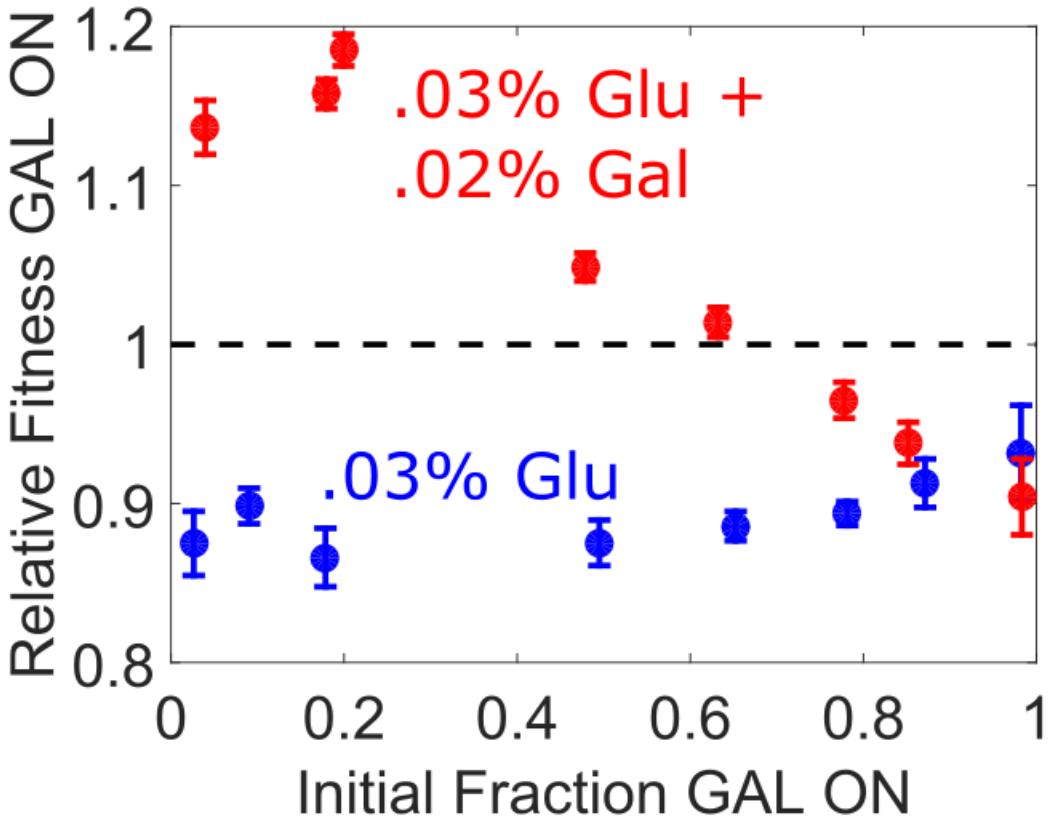

Figure 4.2: Pure strategists show negative frequency dependence under quasi-continuous culture conditions in mixed sugar environment but not pure sugar environment. Pure strategists were mixed in a range of initial fractions in .01% glucose for 24 hours. They were then grown to saturation for 17 hours in either pure glucose (left) or a mixed sugar environment (right). At t=0, 3, 6, and 9 hours, the cells were diluted 2X to replenish with fresh sugars. At t=0, 3, 6, 9, and 12 hours, the fractions of the two strains were measured using flow cytometry. Relative fitness of the two strains is computed using the relative fraction of the two strains at t=0 and t=12 hours. The relative fitness of the galactose strategist is plotted as a function of its initial fraction. Error bars were determined using bootstrap.

Second, we performed evolution experiments in which we showed that in a mixed sugar environment, the pure strategists (either GAL-ON or GAL-OFF) will evolve after approximately 100 generations to a mix of GAL-ON and GAL-OFF cells. This could arise through two distinct mechanisms:

1) The population consists of genetically identical cells, each of which stochastically adopts either a GAL-ON or GAL-OFF phenotype.

2) The population consists of two subpopulations, one of which is GAL-ON and one of which is GAL-OFF.

To distinguish between these two hypotheses, I performed a colony purification on the evolved cells. I streaked cells on an agar plate to get single colonies. I then grew these colonies up in a mixed sugar environment and assayed the activity of their galactose genes using a fluorescent reporter. Interestingly, the two pure strategists took different evolutionary paths to a mixed strategy: the GAL-OFF specialist evolved into a mix of pure strategists, and the GAL-ON specialist evolved into a mixed strategist (Figure 4.3). This is a fascinating observation which we are still seeking to understand mechanistically.

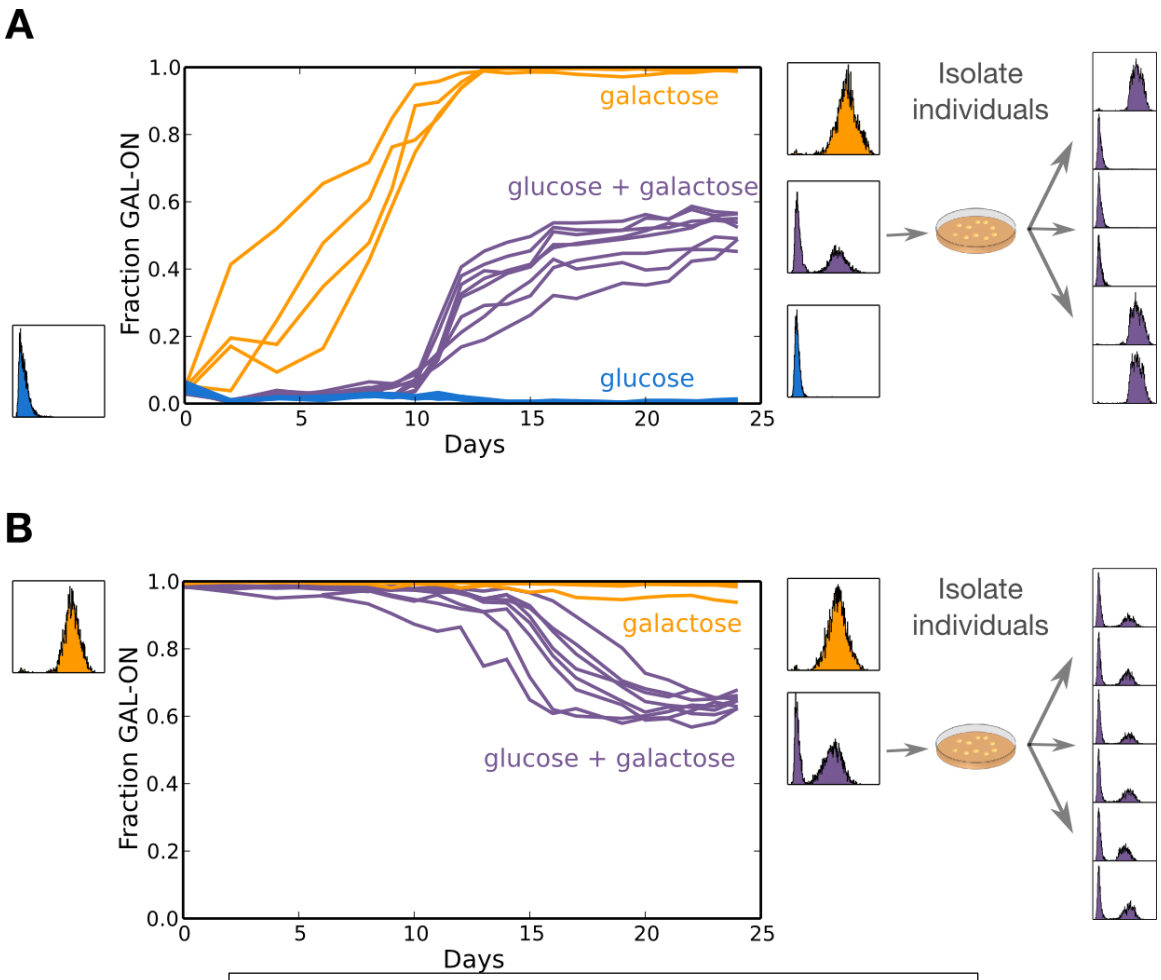

Figure 4.3: Long term evolution of pure strategists

Figure 4.3 (continued): Frequency dependence from a mixed resource environment drives the evolution of both phenotypic and genetic heterogeneity. Eight replicates of each of the two specialist strains (GAL-OFF, **A**, and GAL-ON, **B**) were incubated in the presence of doxycycline and three separate sugar conditions: 0.1% glucose (blue), 0.1% galactose (orange), and a mixture of 0.03% glucose and 0.05% galactose (purple.) Cultures were diluted 1000x daily into fresh media after reaching saturation. To determine the composition of the evolved mixed populations, cultures were plated on agar and individual colonies were assayed for GAL activation in mixed sugars. **A)** Starting from a glucose specialist strain and in the presence of galactose, mutant pure strategist GAL-ON strain arose spontaneously. In pure galactose, the strain eventually took over the population (orange), while in the mixed resource condition, it evolved towards a stable equilibrium with the GAL-OFF strain (right). **B)** Starting from a galactose specialist strain in the presence of mixed sugars, the population similarly evolved to a stable mix of GAL-ON and GAL-OFF, but colony purification revealed that the population had evolved to a clonal population of mixed strategists rather than coexistence of pure strategists. Fraction GAL-ON is not shown for the 1% glucose condition because in that condition, the GAL-ON pure strategist adopts a very low-level unimodal activation state straddling the ON/OFF fluorescence threshold.

4.2 Future Directions and Concluding Remarks

This thesis has explored a range of questions drawn from systems biology and microbial ecology. We have shown some interesting results, but in many cases, we have only begun to scratch the ice. Below, we discuss some caveats and briefly highlight areas for future work.

Cell Memory

For many gene circuits, the threshold for the ON to OFF and OFF to ON transitions occurs at different concentrations of a small molecule inducer. Thus, for intermediate concentrations of inducer, the system can be described as showing memory. However, this is a far cry from showing that bistable gene networks are important memory tools for cellular systems in natural contexts. Even for one of the canonical examples of hysteresis in gene networks, the *E. coli* lactose network, there is some debate as to whether the network is hysteretic in response to changing lactose concentration (most test tube studies use a non-hydrolyzable lactose analog such as Isopropyl β-D-1-thiogalactopyranoside)[76]. Additionally, some computational modeling has indicated that hysteretic mechanisms are neither necessary nor

sufficient for recapitulating observed cell cycle dynamics[77]. This studies cast doubt on how relevant the findings in chapter one will be for natural biological systems. Memory in natural eukaryotic systems may be accomplished through mechanisms other than bistable gene circuits, such as genetic alteration[78].

Another interesting debate revolves around the prediction of impending critical transitions, for which many researchers have been advocating for generic early warning indicators such as critical slowing down[16,17]. However, others in the field have argued that such searches may be a fool's errand[24], because critical slowing down focuses only on local stability and ignores global stability. Some researchers have also advocated for the use of system-specific early warning indicators, rather than generic indicators[79]. Intriguingly, in our gene network, early warning signals based on critical slowing down failed to predict an impending tipping point. Had we used a single cell technique such as microscopy, we could have tested other proposed early warning indicators such as autocorrelation time or flickering[16,80]. Our system presents a unique opportunity to test early warning indicators of critical transitions, particularly systems in which noise can play a significant role in the dynamics. Another attractive feature of our system is that thousands of cells can be probed simultaneously using flow cytometry, which is not possible for tipping points in macroscale systems like lake eutrophication or financial market collapse. It remains to be seen how useful early warning indicators will be in predicting tipping points in real complex systems.

Cross-feeding mutualisms

Our work with a synthetic yeast cross-feeding mutualism highlights that the mode of interaction between two species can be highly dependent on the environmental context. However, one unique aspect of our experimental system is that our two "species" have very

strong niche overlap. In natural mutualisms such as the clownfish and the sea anemone, we would be unlikely to see such a wide range of interaction regimes[33]. For example, it is hard to imagine that those species would ever display competitive exclusion, because they occupy different niches in the ecosystem. Our simple model system with one adjustable parameter is undoubtedly an oversimplification of the complex interactions seen in natural ecosystems. Yet, there are reasons to believe that our results could be broadly relevant, particularly in microbial communities such as soil or the human microbiome where nutrient interdependencies are quite common[81,82]. Microbial cross-feeding will be an exciting area of exploration in coming years.

Again, the topic of early warning indicators of bifurcations reared its head in this study. One of our goals when we set out was to measure fluctuations in N_1 versus N_2 space and determine whether the dominant fluctuations were along the axis connecting a stable fixed point to extinction, or whether the dominant fluctuations were perpendicular to the aforementioned axis. We hypothesized that the dominant axis of fluctuations might shift as we supplemented with different quantities of amino acids, and that the shift in the fluctuation axis could be used as an early warning indicator of system collapse. However, we were unable to characterize the fluctuations with sufficient resolution to address this question. On a related note, our lab is currently using these synthetic yeast cross-feeding strains to test a novel early warning indicator of an impending bifurcation: reactivity[83]. Preliminary results from these studies should be available later in 2016.

One of the most useful outcomes from this study was a simple yet successful mathematical model for describing the dynamics of cross-feeding mutualisms. This is sorely needed in the field, because the standard go-to framework, Lotka-Volterra, yields nonsensical

results where population sizes diverge to infinite in some regimes[84]. We hope that future work will further validate this model and prove useful for other researchers.

The Allee effect and Evolutionary Rescue

One major assumption underlying our work in this area is that Allee effects are common in nature. There are plenty of well-grounded reasons, both theoretical and experimental, why this would be the case. Populations which engage in collective hunting behaviors will logically struggle to hunt if there are too few members of a population to track prey. Assaying for an Allee effect in a population involves measuring the population growth rate at different population sizes. Given the inherent difficulties of measuring both these quantities in field ecology studies, we must take any claims of Allee effects in natural populations with a grain of salt.

One other important consideration is the timescale of evolutionary rescue: beneficial mutants need time to sweep through populations. In our experiments, rescue trajectories from decline to recovery often took tens of generations. For natural populations which take years to reach sexual maturity, evolutionary rescue might require decades or centuries, which might be too slow in light of the current rate of climate change. We have dealt here only with well-mixed populations where migration to a region of better habitat was not an option; future studies should study how an Allee effect influences the probability of evolutionary rescue in a spatially extended population. In contrast to evolutionary rescue by altering genomic structure, phenotypic adaptation (when possible) likely represents a more expedient route to survival in harsh environments. An idea that has always fascinated me is the concept of phenotypic plasticity: might evolution select for individuals which are able to adopt a wide range of phenotypes[85]?

The Allee effect / evolutionary rescue study is one project in our lab's larger effort to understand how cooperative interactions can alter microbial ecological and evolutionary

dynamics[86–88]. Ongoing work in our lab has shown that cooperative interactions in spatially expanding populations can result in a so-called "pushed" wave, whereas non-cooperatively growing expanding populations expand as a "pulled" wave. Future work will continue to elucidate the deep significance of cooperative interactions in microbial ecology.

References

1. Hu, J., Qin, K. R., Xiang, C. & Lee, T. H. Modeling of hysteresis in gene regulatory networks. *Bull. Math. Biol.* **74,** 1727–1753 (2012).

2. Williams, K., Savageau, M. A. & Blumenthal, R. M. A bistable hysteretic switch in an activator–repressor regulated restriction–modification system. *Nucleic Acids Res.* gkt324 (2013).

3. Ozbudak, E. M., Thattai, M., Lim, H. N., Shraiman, B. I. & Van Oudenaarden, A. Multistability in the lactose utilization network of Escherichia coli. *Nature* **427,** 737–740 (2004).

4. Acar, M., Becskei, A. & van Oudenaarden, A. Enhancement of cellular memory by reducing stochastic transitions. *Nature* **435,** 228–232 (2005).

5. Chen, D. *et al.* Global transcriptional responses of fission yeast to environmental stress. *Mol. Biol. Cell* **14,** 214–229 (2003).

6. Gasch, A. P. & Werner-Washburne, M. The genomics of yeast responses to environmental stress and starvation. *Funct. Integr. Genomics* **2,** 181–192 (2002).

7. Gasch, A. P. *et al.* Genomic expression programs in the response of yeast cells to environmental changes. *Mol. Biol. Cell* **11,** 4241–4257 (2000).

8. Brauer, M. J. *et al.* Coordination of growth rate, cell cycle, stress response, and metabolic activity in yeast. *Mol. Biol. Cell* **19,** 352–367 (2008).

9. Igoshin, O. A., Price, C. W. & Savageau, M. A. Signalling network with a bistable hysteretic switch controls developmental activation of the σF transcription factor in Bacillus subtilis. *Mol. Microbiol.* **61,** 165–184 (2006).

10. Kotula, J. W. *et al.* Programmable bacteria detect and record an environmental signal in the mammalian gut. *Proc. Natl. Acad. Sci.* **111,** 4838–4843 (2014).

11. Ajo-Franklin, C. M. *et al.* Rational design of memory in eukaryotic cells. *Genes Dev.* **21,** 2271–2276 (2007).

12. Xiong, W. & Ferrell, J. E. A positive-feedback-based bistable 'memory module'that governs a cell fate decision. *Nature* **426,** 460–465 (2003).

13. Angeli, D., Ferrell, J. E. & Sontag, E. D. Detection of multistability, bifurcations, and hysteresis in a large class of biological positive-feedback systems. *Proc. Natl. Acad. Sci. U. S. A.* **101,** 1822–1827 (2004).

14. Ferrell, J. E. & Machleder, E. M. The biochemical basis of an all-or-none cell fate switch in Xenopus oocytes. *Science* **280,** 895–898 (1998).

15. Pomerening, J. R., Sontag, E. D. & Ferrell, J. E. Building a cell cycle oscillator: hysteresis and bistability in the activation of Cdc2. *Nat. Cell Biol.* **5,** 346–351 (2003).

16. Dai, L., Vorselen, D., Korolev, K. S. & Gore, J. Generic indicators for loss of resilience before a tipping point leading to population collapse. *Science* **336,** 1175–1177 (2012).

17. Scheffer, M. *et al.* Early-warning signals for critical transitions. *Nature* **461,** 53–59 (2009).

18. Ellis, T., Wang, X. & Collins, J. J. Diversity-based, model-guided construction of synthetic gene networks with predicted functions. *Nat. Biotechnol.* **27,** 465–471 (2009).

19. Gardner, T. S., Cantor, C. R. & Collins, J. J. Construction of a genetic toggle switch in Escherichia coli. *Nature* **403,** 339–342 (2000).

20. Wu, M. *et al.* Engineering of regulated stochastic cell fate determination. *Proc. Natl. Acad. Sci.* **110,** 10610–10615 (2013).

21. Blake, W. J. *et al.* Phenotypic consequences of promoter-mediated transcriptional noise. *Mol. Cell* **24,** 853–865 (2006).

22. Van Nes, E. H. & Scheffer, M. Slow recovery from perturbations as a generic indicator of a nearby catastrophic shift. *Am. Nat.* **169,** 738–747 (2007).

23. Isaacs, F. J., Hasty, J., Cantor, C. R. & Collins, J. J. Prediction and measurement of an autoregulatory genetic module. *Proc. Natl. Acad. Sci.* **100,** 7714–7719 (2003).

24. Menck, P. J., Heitzig, J., Marwan, N. & Kurths, J. How basin stability complements the linear-stability paradigm. *Nat. Phys.* **9,** 89–92 (2013).

25. Biggar, S. R. & Crabtree, G. R. Cell signaling can direct either binary or graded transcriptional responses. *EMBO J.* **20,** 3167–3176 (2001).

26. Song, C. *et al.* Estimating the stochastic bifurcation structure of cellular networks. *PLoS Comput Biol* **6,** e1000699 (2010).

27. Gancedo, J. M. Yeast carbon catabolite repression. *Microbiol. Mol. Biol. Rev.* **62,** 334–361 (1998).

28. Gillespie, D. T. Exact stochastic simulation of coupled chemical reactions. *J. Phys. Chem.* **81,** 2340–2361 (1977).

29. Choi, P. J., Cai, L., Frieda, K. & Xie, X. S. A stochastic single-molecule event triggers phenotype switching of a bacterial cell. *Science* **322,** 442–446 (2008).

30. Thébault, E. & Fontaine, C. Stability of ecological communities and the architecture of mutualistic and trophic networks. *Science* **329,** 853–856 (2010).

31. Rohr, R. P., Saavedra, S. & Bascompte, J. On the structural stability of mutualistic systems. *Science* **345,** 1253497 (2014).

32. Klein, A.-M. *et al.* Importance of pollinators in changing landscapes for world crops. *Proc. R. Soc. Lond. B Biol. Sci.* **274,** 303–313 (2007).

33. Fautin, D. G. The anemonefish symbiosis: what is known and what is not. (1991).

34. Cordes, E. E., Arthur, M. A., Shea, K., Arvidson, R. S. & Fisher, C. R. Modeling the mutualistic interactions between tubeworms and microbial consortia. *PLoS Biol* **3,** e77 (2005).

35. Bronstein, J. L. Our current understanding of mutualism. *Q. Rev. Biol.* 31–51 (1994).

36. Chamberlain, S. A., Bronstein, J. L. & Rudgers, J. A. How context dependent are species interactions? *Ecol. Lett.* **17,** 881–890 (2014).

37. Palmer, T. M. *et al.* Breakdown of an ant-plant mutualism follows the loss of large herbivores from an African savanna. *Science* **319,** 192–195 (2008).

38. Liu, J. *et al.* Metabolic co-dependence gives rise to collective oscillations within biofilms. *Nature* **523,** 550–554 (2015).

39. Shou, W., Ram, S. & Vilar, J. M. Synthetic cooperation in engineered yeast populations. *Proc. Natl. Acad. Sci.* **104,** 1877–1882 (2007).

40. Müller, M. J., Neugeboren, B. I., Nelson, D. R. & Murray, A. W. Genetic drift opposes mutualism during spatial population expansion. *Proc. Natl. Acad. Sci.* **111,** 1037–1042 (2014).

41. Mee, M. T., Collins, J. J., Church, G. M. & Wang, H. H. Syntrophic exchange in synthetic microbial communities. *Proc. Natl. Acad. Sci.* **111,** E2149–E2156 (2014).

42. Vetsigian, K., Jajoo, R. & Kishony, R. Structure and evolution of Streptomyces interaction networks in soil and in silico. *PLoS Biol* **9,** e1001184 (2011).

43. Waite, A. J. & Shou, W. Adaptation to a new environment allows cooperators to purge cheaters stochastically. *Proc. Natl. Acad. Sci.* **109,** 19079–19086 (2012).

44. Hom, E. F. & Murray, A. W. Niche engineering demonstrates a latent capacity for fungal-algal mutualism. *Science* **345,** 94–98 (2014).

45. Wintermute, E. H. & Silver, P. A. Emergent cooperation in microbial metabolism. *Mol. Syst. Biol.* **6,** 407 (2010).

46. Hosoda, K. *et al.* Cooperative adaptation to establishment of a synthetic bacterial mutualism. *PLoS One* **6,** e17105 (2011).

47. Akashi, H. Translational selection and yeast proteome evolution. *Genetics* **164,** 1291–1303 (2003).

48. Hardin, G. The competitive exclusion principle. *science* **131,** 1292–1297 (1960).

49. Kot, M. *Elements of mathematical ecology*. (Cambridge University Press, 2001).

50. Callaway, R. M. *et al.* Positive interactions among alpine plants increase with stress. *Nature* **417,** 844–848 (2002).

51. Johnson, N. C., Graham, J.-H. & Smith, F. A. Functioning of mycorrhizal associations along the mutualism–parasitism continuum. *New Phytol.* **135,** 575–585 (1997).

52. Karst, J., Marczak, L., Jones, M. D. & Turkington, R. The mutualism-parasitism continuum in ectomycorrhizas: a quantitative assessment using meta-analysis. *Ecology* **89,** 1032–1042 (2008).

53. Thomas, C. D. *et al.* Extinction risk from climate change. *Nature* **427,** 145–148 (2004).

54. Carpenter, K. E. *et al.* One-third of reef-building corals face elevated extinction risk from climate change and local impacts. *Science* **321,** 560–563 (2008).

55. Gomulkiewicz, R. & Holt, R. D. When does evolution by natural selection prevent extinction? *Evolution* **49,** 201–207 (1995).

56. Lynch, M. & Lande, R. Evolution and extinction in response to environmental change. *Biot. Interact. Glob. Change* 234–250 (1993).

57. Orr, H. A. & Unckless, R. L. Population extinction and the genetics of adaptation. *Am. Nat.* **172,** 160–169 (2008).

58. De Mazancourt, C., Johnson, E. & Barraclough, T. G. Biodiversity inhibits species' evolutionary responses to changing environments. *Ecol. Lett.* **11,** 380–388 (2008).

59. Bell, G. & Gonzalez, A. Evolutionary rescue can prevent extinction following environmental change. *Ecol. Lett.* **12,** 942–948 (2009).

60. Bell, G. & Gonzalez, A. Adaptation and evolutionary rescue in metapopulations experiencing environmental deterioration. *Science* **332,** 1327–1330 (2011).

61. Low-Décarie, E. *et al.* Community rescue in experimental metacommunities. *Proc. Natl. Acad. Sci.* **112,** 14307–14312 (2015).

62. Lindsey, H. A., Gallie, J., Taylor, S. & Kerr, B. Evolutionary rescue from extinction is contingent on a lower rate of environmental change. *Nature* **494,** 463–467 (2013).

63. Hao, Y.-Q., Brockhurst, M. A., Petchey, O. L. & Zhang, Q.-G. Evolutionary rescue can be impeded by temporary environmental amelioration. *Ecol. Lett.* **18,** 892–898 (2015).

64. Allee, W. C. Animal aggregations. (1931).

65. Kramer, A. M., Dennis, B., Liebhold, A. M. & Drake, J. M. The evidence for Allee effects. *Popul. Ecol.* **51,** 341–354 (2009).

66. Cappuccino, N. Allee effect in an invasive alien plant, pale swallow-wort Vincetoxicum rossicum (Asclepiadaceae). *Oikos* **106,** 3–8 (2004).

67. Clutton-Brock, T. H. *et al.* Predation, group size and mortality in a cooperative mongoose, Suricata suricatta. *J. Anim. Ecol.* **68,** 672–683 (1999).

68. Kramer, A. M., Sarnelle, O. & Knapp, R. A. Allee effect limits colonization success of sexually reproducing zooplankton. *Ecology* **89,** 2760–2769 (2008).

69. Gore, J., Youk, H. & Van Oudenaarden, A. Snowdrift game dynamics and facultative cheating in yeast. *Nature* **459,** 253–256 (2009).

70. Blank, L. M. & Sauer, U. TCA cycle activity in Saccharomyces cerevisiae is a function of the environmentally determined specific growth and glucose uptake rates. *Microbiology* **150,** 1085–1093 (2004).

71. Albertyn, J., Hohmann, S., Thevelein, J. M. & Prior, B. A. GPD1, which encodes glycerol-3-phosphate dehydrogenase, is essential for growth under osmotic stress in Saccharomyces cerevisiae, and its expression is regulated by the high-osmolarity glycerol response pathway. *Mol. Cell. Biol.* **14,** 4135–4144 (1994).

72. Filteau, M. *et al.* Evolutionary rescue by compensatory mutations is constrained by genomic and environmental backgrounds. *Mol. Syst. Biol.* **11,** 832 (2015).

73. Mace, G. M. & Lande, R. Assessing extinction threats: toward a reevaluation of IUCN threatened species categories. *Conserv. Biol.* **5,** 148–157 (1991).

74. Kussell, E. & Leibler, S. Phenotypic diversity, population growth, and information in fluctuating environments. *Science* **309,** 2075–2078 (2005).

75. Veening, J.-W. *et al.* Bet-hedging and epigenetic inheritance in bacterial cell development. *Proc. Natl. Acad. Sci.* **105,** 4393–4398 (2008).

76. Díaz-Hernández, O. & Santillán, M. Bistable behavior of the lac operon in E. coli when induced with a mixture of lactose and TMG. *Front. Physiol.* **1,** (2010).

77. Han, Z., Yang, L., MacLellan, W. R., Weiss, J. N. & Qu, Z. Hysteresis and cell cycle transitions: how crucial is it? *Biophys. J.* **88,** 1626–1634 (2005).

78. Hozumi, N. & Tonegawa, S. Evidence for somatic rearrangement of immunoglobulin genes coding for variable and constant regions. *Proc. Natl. Acad. Sci.* **73,** 3628–3632 (1976).

79. Boettiger, C. & Hastings, A. Tipping points: From patterns to predictions. *Nature* **493,** 157–158 (2013).

80. Wang, R. *et al.* Flickering gives early warning signals of a critical transition to a eutrophic lake state. *Nature* **492,** 419–422 (2012).

81. Qiu, Q., Conrad, R. & Lu, Y. Cross-feeding of methane carbon among bacteria on rice roots revealed by DNA-stable isotope probing. *Environ. Microbiol. Rep.* **1,** 355–361 (2009).

82. Belenguer, A. *et al.* Two routes of metabolic cross-feeding between Bifidobacterium adolescentis and butyrate-producing anaerobes from the human gut. *Appl. Environ. Microbiol.* **72,** 3593–3599 (2006).

83. Caswell, H. & Neubert, M. G. Reactivity and transient dynamics of discrete-time ecological systems. *J. Differ. Equ. Appl.* **11,** 295–310 (2005).

84. Iwata, S., Kobayashi, K., Higa, S., Yoshimura, J. & Tainaka, K. A simple population theory for mutualism by the use of lattice gas model. *Ecol. Model.* **222,** 2042–2048 (2011).

85. Via, S. *et al.* Adaptive phenotypic plasticity: consensus and controversy. *Trends Ecol. Evol.* **10,** 212–217 (1995).

86. Ratzke, C. & Gore, J. Self-organized patchiness facilitates survival in a cooperatively growing Bacillus subtilis population. *Nat. Microbiol.* 16022 (2016).

87. Artemova, T., Gerardin, Y., Dudley, C., Vega, N. M. & Gore, J. Isolated cell behavior drives the evolution of antibiotic resistance. *Mol. Syst. Biol.* **11,** 822 (2015).

88. Datta, M. S., Korolev, K. S., Cvijovic, I., Dudley, C. & Gore, J. Range expansion promotes cooperation in an experimental microbial metapopulation. *Proc. Natl. Acad. Sci.* **110,** 7354–7359 (2013).